POLITECNICO DI TORINO

MASTER THESIS

Nanowire biosensor as cost-effective testing platform for biomedical applications

Author:
Lorenzo LOMBARDO

Supervisor:
Dr. Matteo COCUZZA
Dr. Sergio FERRERO
Project Internship Supervisor,
Trinity College Dublin:
Dr. Adriele PRINA-MELLO

A thesis submitted in fulfillment of the requirements for the degree of Nanotechnologies for ICTs

September 10, 2018

POLITECNICO DI TORINO

Abstract

Nanotechnologies for ICTs

Nanowire biosensor as cost-effective testing platform for biomedical applications

by Lorenzo LOMBARDO

Devices based on nanostructures, such as nanogaps and nanowires, are widely employed in bio-sensing, for example building a sensing nanowire structure on a nanogap between two electrodes. The main difficulty in the fabrication process of these structures is due to the fact that the nanogap between the electrode is created starting from a continuous structure and then using electromigration, but this process is random and so non-controllable. Moreover the positioning of the nanowire right in the middle of the gap is quite challenging. In this work, starting from the fabrication of the devices (based on a previous work and slightly modified), different tests on the devices are performed, starting from measuring the resistance of the nanowire itself, to a detection of human fibrinogen. These particular molecules, are widely studied in medical sciences because of their central role in human immune response, helping to stop excessive bleeding when an injury happens. The best way to do fibrinogen detection is through an ELISA kit, but these kits are quite big and so less sensitive than a nanostructure-based biosensor. A better approach, that is followed in this work, is to employ a nanostructure, such as a nanowire, in order to obtain a better sensitivity and a better specificity, with a cost-effective solution. In this approach the biological readouts are achieved by relative measurement of the fibrinogen binding on the surface of the functionalised nanowire surface. Readouts in this instance are achieved as I/V curves within the linear resistance response of the sensor. This enables to achieve sensitivity but also additional specificity when the functionalisation is successful. The characterisation and battery of results achieved in this thesis are showing promising evidence for biomedical applications in the haematology rapid detection diagnostic area.

Acknowledgements

First of all I want to thank my supervisors, Dr. Matteo Cocuzza and Dr. Sergio Ferrero. They helped me a lot during the period I spent at Trinity College, supporting me and helping me with technical issues I experienced.

A huge thank you to my project internship supervisor in Dublin, Dr. Adriele Prina-Mello, that gave me the opportunity to work in his lab and under his supervision. He welcomed me in his group and helped me understanding a lot of topics, present in my thesis, that are completely new to me, because of my background, mostly in electronics. He was a great point of reference for me, he was so patient with me even when I wanted to do things my way (that was most of the times the worst way) and most of all he sustained me when I experienced issues in my project.

A special thanks to prof. Alessandro Sanginario, who sent me the masks and gave me all the details about the fabrication process.

Thanks a lot to all the people from Trinity College, in particularly from CRANN, that helped me developing my project. Thanks to Ivan (I would not have done all this work without your help), Fabio, Giulio, Julia, Peter, Ajay, Cormac, Dermot, Eoin, Megan and Gwaenel. I am forgetting someone of course, but I really appreciated your help for training and for all the steps I needed to perform for my project.

Thanks also to the Nanomedicine team: Anna, Melissa, Kieran, Gary, Monica and Michela. Even if you were not so familiar with engineering, you gave me your help with all the "bio-stuff" and, most important, you welcomed me in your group as colleagues and friends. I am gonna miss you.

The last thank you is for my family: mom, dad, Alby and Francy. You supported me in every moment, you helped me with my (frequent) anxiety and you were a continuous point of reference, even with a great distance between us.

Contents

List of Figures

List of Tables

List of Abbreviations

FIB	**F**ocused **I**on **B**eam
SOI	**S**ilicon **O**n **I**nsulator
AuNWA	Gold **N**ano **W**ire **A**rray
GLA	**GL**utar**A**ldehyde
BSA	**B**ovine **S**erum **A**lbumin
HRP	**H**orse**R**adish **P**eroxidase
SEM	**S**canning **E**lectron **M**icroscope
APTT	**A**ctivated **P**artial **T**hromboplastin **T**ime
QCM	**Q**uartz **C**rystal **M**icrobalance
HEMT	**H**igh **E**lectron **M**obility **T**ransistor
SWCNT	**S**ingle **W**alled **C**arbon **N**ano**T**ube
POC	**P**oint **O**f **C**are
PCB	**P**rinted **C**ircuit **B**oard
CZ	**CZ**ochralski
RF	**R**adio **F**requency
DI Water	**DeI**onized Water
IPA	**I**so**P**rop**A**nol
PBS	**P**hosphate-**B**uffered **S**aline
DSU	**Di**-thio-bis- **S**uccinimidyl**U**ndecanoate
ELISA	**E**nzyme-**L**inked **I**mmuno**S**orbent **A**ssay

Chapter 1

Introduction and Literature Review

1.1 Introduction

Nanogap devices are widely employed in biosensors, to detect nanometric-scale substances, like molecules and cells: a gap is created between two electrodes and then the particles are put in it. Then the electrodes are electrically stimulated and the reaction of the molecules to the applied voltage can be measured.

The main issue with these kind of devices is the fabrication part, because the gap is normally created by electromigration; in this way the width cannot be controlled, it is random. Moreover, in some cases a nanowire is added onto the gap to have a more sensitive detection: performing a precise positioning of this wire is again very challenging with the current technology.

In this work, after a literature review on devices based on nanogaps and nanowires and specifically on fibrinogen and blood components detection, a novel approach to the creation of this structure is described, based on a NANOfab (instrument composed by 3 different FIBs) treatment. Instead of creating the gap and then bridge it with a nanowire, after the fabrication part the bridge between the electrodes is thinned with the NANOfab. After the FIBbing, the devices can be tested: the first step is to do a preliminary sensor calibration measuring the resistance of the nanowires in air, water and PBS (a saline solution), to check if the devices are working properly. Then the nanowires are functionalized, to make the surface capable of binding fibrinogen molecules and three different measurements of resistance are performed: first on the functionalized devices without anything

on top, second on the functionalized devices with fibrinogen bound on the surface and finally on functionalized devices with fibrinogen and a blood single droplet on it.

1.2 Literature review

1.2.1 Nanogap devices

In the first part of the literature review the state of the art in nanogap-based devices is analyzed.

Nanogap devices are currently used for the detection of very small substances, invisible to human eye, mostly bio-molecules. Since the size of this molecules is around a few nanometers, a very small structure is needed to achieve a good sensitivity, even with a small number of molecules. Another great advantages of these kind of sensors are the compatibility with semiconductor technology and low cost of production. The main challenges, instead, are the integration, the miniaturization (that can require complex technologies) and mostly the cost of production [1].

Another main advantage of these structures, compared to classical biosensors, is that they don't always need labels, that can be challenging to prepare and they can interfere with the sensing itself. Moreover, another advantage is the possibility to have a real-time monitoring of the reactions of the molecules; the detection is performed through a transduction from a binding event at molecule level to an electrical event at the electrode level, like a change of impedance, current or voltage [1].

Together with label-free nanogaps, they can be nanoparticle-labeled or even bridged with nanowires and nanotubes, depending on the type of sensing needed: this gives rise to a wide spread of possible solutions, depending on the application needed [1].

Nanogap devices for biosensing can be divided into two main categories: planar devices and vertical devices.

Planar nanogap devices

Planar nanogap devices are basically composed by two electrodes in front of each other, on top of an horizontal device.

An example of a planar nanogap device (fig. 1.1 a), based on carbon nanotube electrodes, is reported by Roy et al. [2]. The devices is composed by two carbon nanotube electrodes, between which a DNA strand is immobilized (fig. 1.1 b): the functioning is very simpled and it is basically based on a change of conductance between the structure without the DNA in the middle and the structure with the DNA connecting the two electrodes. When a double strand DNA connects the electrodes a current of around (25 to 40) pA is measured (fig. 1.1 c), while with a single strand DNA the current detected is below 1 pA, due to an irregular stacking on nucleotide basis (fig. 1.1 d).

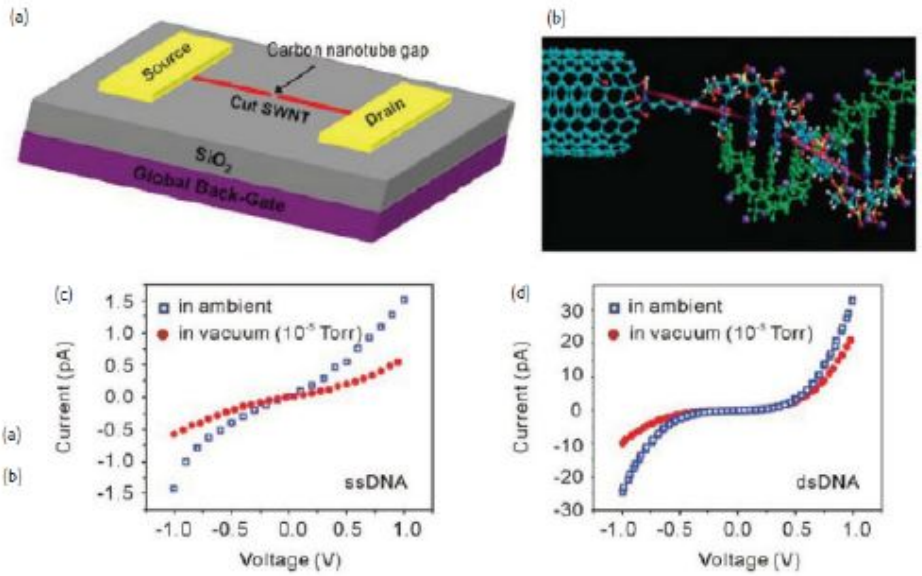

FIGURE 1.1: SWCNT planar nanogap devices. a) devices structure b) bond between the SWCNT and the DNA strand c) and d) I-V curves of the DNA-gapped device (source: [2])

A nanogap-based sensor for electrical detection of bio-molecules was realized by Kim et al. [3]. The particular trapezoidal structure of the nanogap (fig. 1.2 a) is obtained thanks of a wet anisotropic etching of a SOI wafer. The operation of the device is simple: when a bond between a pair of molecules, such as antibody/antigen (fig. 1.2 b), happens, it

results in an increase of current, that can be detected. Depending on the concentration of the molecules, the current increases in the range of 100 fg mL^{-1} and 100 ng mL^{-1} at 1 V bias (fig. 1.2 c and d).

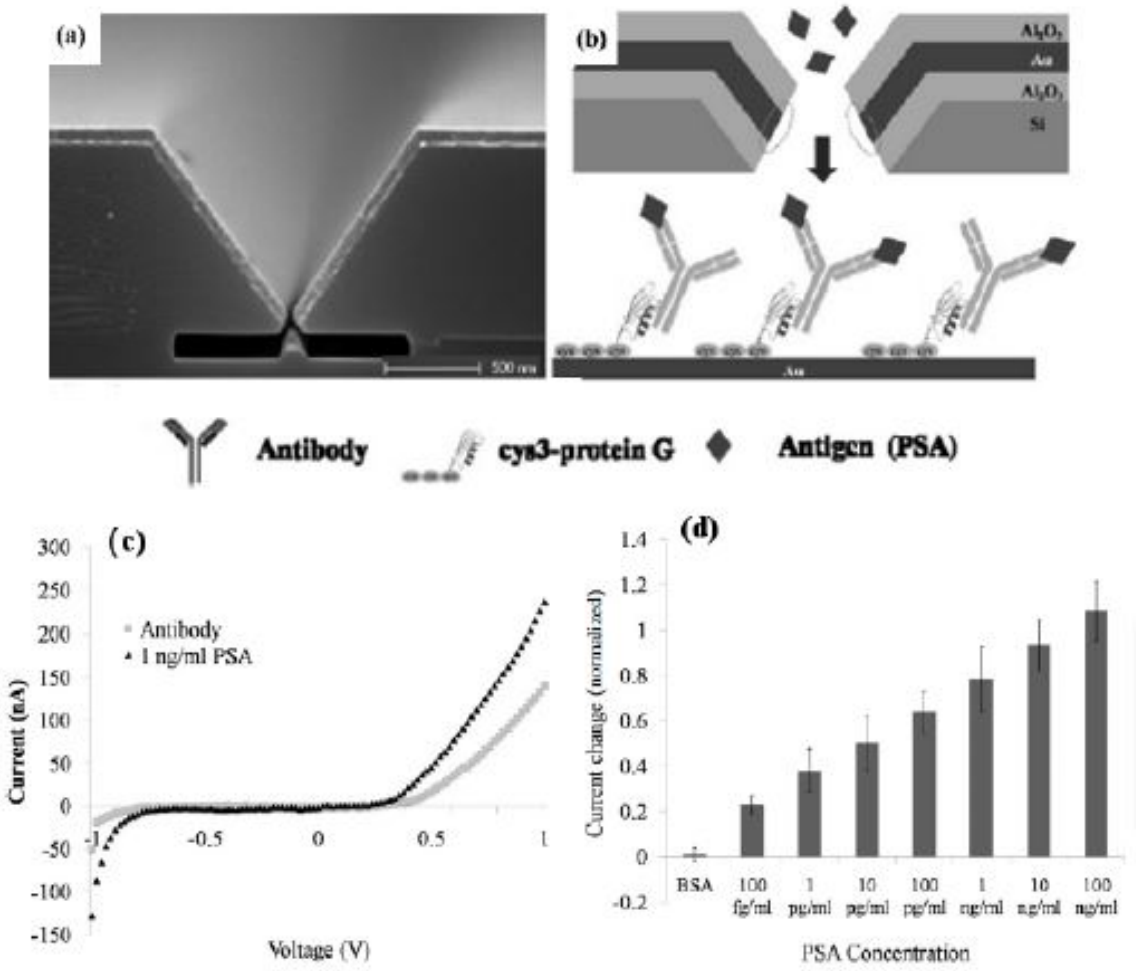

FIGURE 1.2: Trapezoidal planar nanogap devices. a) devices structure b) molecular interaction inside the gap c) I-V curves d) signal intensity versus concentration of the molecules (source: [3])

One last example of planar nanogap devices is reported by McCarthy et al. [4]: they designed a nanogap device for detection of dopamine in aqueous solution (fig. 1.3). The device is an electrochemical cell composed by the two nanogap electrodes as counter and working electrode and an external reference electrode. The two redox peaks that appear were related to the concentration of dopamine through the oxidation and reduction of the

analyte to and from dopamine-o-quinone. The study enlightened the scaling effect, showing that cycling of active molecules at the confined geometry of the nanogap, involving the measure of just a few molecules, gives a large enhancement of the signal intensity.

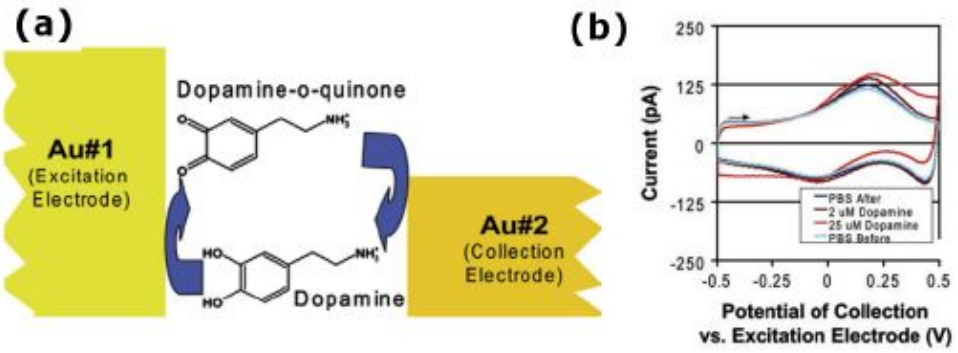

FIGURE 1.3: Nanogap device for dopamine detection. a) device structure b) I-V curves (source: [4])

Vertical nanogap devices

Vertical nanogap devices are composed by two electrodes in a vertical configuration, one on top of the other, with the gap in the middle.

An early example is again a work by Roy et al . [5], that reports a nanogap-based array for the detection of DNA: this bionsensor is composed by two gold electrodes, separated by a SiO_2 insulating layer (fig. 1.4). Two capture probes are located on the two electrodes, one on the top one and one on the bottom one. The two capture probes are connected, bridging the nanogap, through an hybridization mechanism and then a metallization step (with silver) follows, in order to have a path for the electric current to flow. In this way a difference of conductivity between the devices with no DNA (resulting in no metallic connection) among the electrodes and devices that hybridize successfully can be detected. This difference in conductance is quite large (about 2 orders of magnitude), even with a very small concentration of DNA (1 fmol).

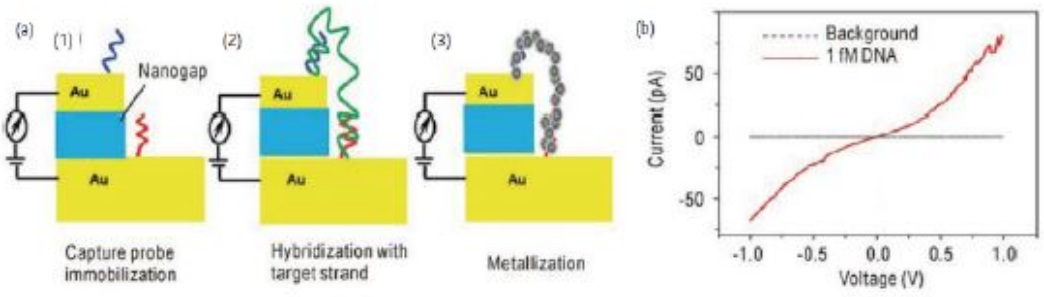

FIGURE 1.4: Vertical nanogap devices and sensing procedure. a) capture probe immobilization on the electrodes b) hybridization c) metallization of the DNA strand with silver d) I-V curve of the DNA-gapped device (source: [5])

1.2.2 Nanowire devices

Together with biosensors based on nanogaps, nanowire-based devices play a fundamental role on the detection of molecules, thanks to their small dimensions that assure a very high sensitivity. Gold is one of the preferred materials thanks to its great conductivity and biocompatibility [6].

Lu et al. [7] realized enzyme-functionalized gold nanowires for the fabrication of biosensors. In their work they employ electrodeposition to deposit gold nanowires (fig. 1.5 a), with dimensions around 250 nm in width x 10 µm in length, in polycarbonate membrane and then dispersed into chitosan and immobilized. The electrode modified with nanowires is found to have a more sensitive response towards hydrogen peroxide with respect to a conventional gold one. This high sensitivity makes the modified electrode ideal for the absorption of enzymes, in order to create biosensing devices. Glucose oxidase was selected and absorbed onto the gold nanowire surface, and the resulting glucose biosensor enables selective determination of glucose with high sensitivity and wide linear range (fig. 1.5 b).

Another example of biosensors based on gold nanowires is reported in Hui et al. [8]: a hybrid flow injection-nanobiosensor system for the detection of glucose at low potential is presented in this paper. For the fabrication of the biosensor, highly ordered AuNWAs are synthesized by direct electrodeposition (fig. 1.6). Glucose oxidase and horseradish peroxidase are immobilized on the surface of the resultant gold nanowire

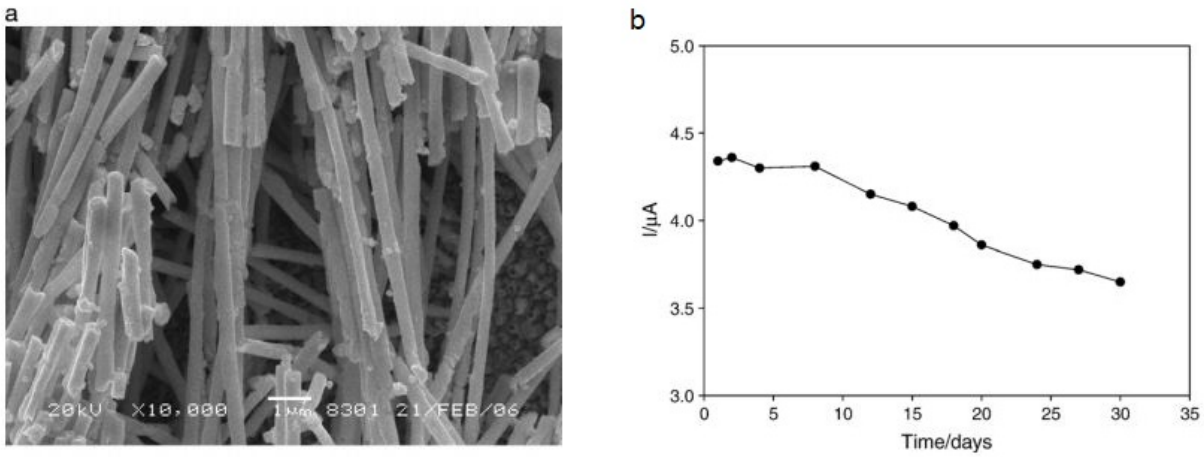

FIGURE 1.5: a) SEM image of gold nanowires b) Long term stability of the glucose biosensor toward 1 mM glucose (source: [7])

arrays by cross-linking with GLA and BSA. In combination with a flow injection system, the biosensor demonstrates high performance in glucose detection with a sensitivity of 25.34 µA cm^{-2} $mmol^{-1}$, a linear range between 5 and 1000 µmol and a detection limit of 1 µmol. High selectivity is achieved together with good reproducibility, repeatability and stability, which are beneficial for the practical applications in glucose detection. Finally, the developed nanobiosensor is applied to the detection of glucose in river water and the biosensor presents good performance.

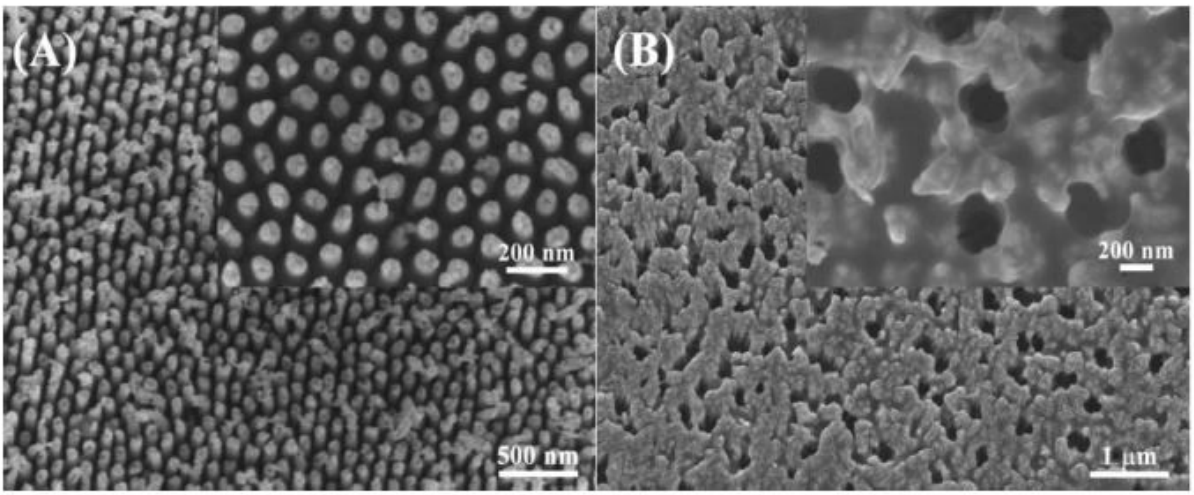

FIGURE 1.6: a) SEM image of gold nanowires without modification a) and modified with HRP b) (source: [8])

1.2.3 Fibrinogen detection

Fibrinogen detection plays a fundamental role in the area of biosensing, due to the great importance of this molecules in medical sciences and biology. In fact having the possibility to detect, when the concentration of fibrinogen in a sample is known, its interaction with human blood (fibrinogen can bind to trombin or fibrin and be activated [9]) can give important information about the blood coagulation, fundamental in the study of haemostatic disorders.

Moreover performing the detection on a portable device, equipped with a nanotechnology based biosensor, can give the possibility to have a real time detection, with a cost-effective solution.

Poon et al. [10] employed Raman spectroscopy to detect fibrinogen levels in human plasma. Raman spectroscopy has been applied to the analysis of blood for years to determine various analyte concentrations such as glucose, urea, triglycerides and cholesterol. In this study, Raman spectroscopy is employed to quantify fibrinogen concentration in blood plasma. Samples collected from 34 patients are analyzed by Raman spectroscopy and the resultant spectra are fitted with a Partial Least Squares Regression model. Various spectral pre-processing methods are utilized to prepare data to be entered into a calibration model. A root mean square error of prediction of $(0.72 \pm 0.05)\,\mathrm{g\,L^{-1}}$ is achieved with as few as 25 spectra. In this pilot study, Raman spectroscopy has been demonstrated to be a robust technique providing rapid and reagent-free quantification of fibrinogen levels in blood plasma.

A study by Yao et al. [11] presents a Quartz crystal microbalance biosensor, with nanogram sensitivity, for the detection of fibrinogen and coagulation factor VIII, an important parameter in the study of haemostatic diseases, like thrombosis or hemophilia A. The device is used to determine the APTT for 120 anticoagulated plasma specimens. A good linear relationship is found in APTT versus fibrinogen concentration plot, in the range of $(1.58$ to $6.30)\,\mathrm{g\,L^{-1}}$. For factor VIII, the detection range by the QCM biosensor is $(0.0185$ to $0.111)\,\mathrm{mg\,L^{-1}}$. The QCM biosensor results were compared with those obtained

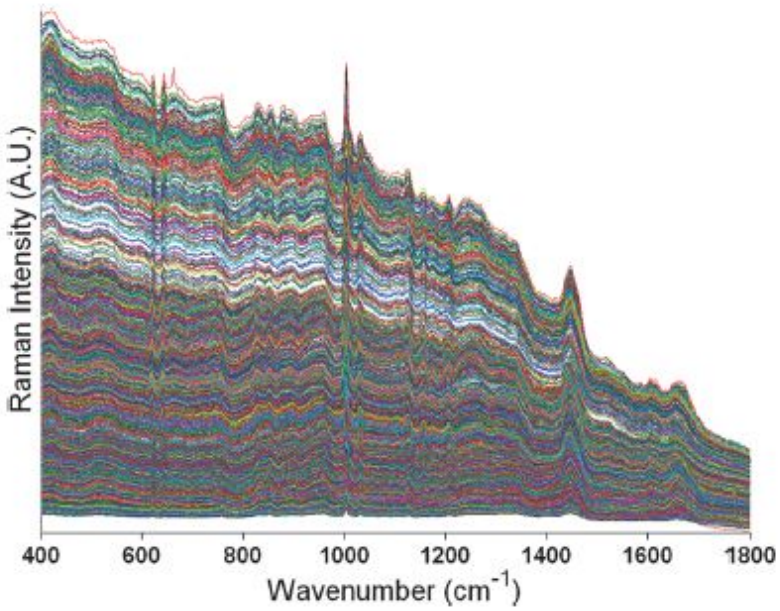

FIGURE 1.7: Raman spectra (n=3400) obtained from human blood plasma sample (source: [10])

by commercial optical coagulometry and a good correlation coefficient was reached. Furthermore, the QCM determination can be completed within 10 min, demonstrating the potential in real-time diagnostics.

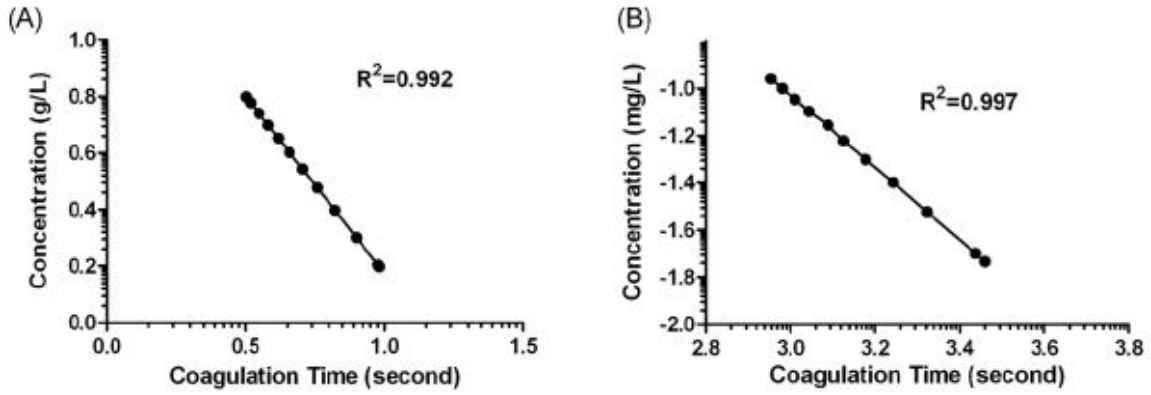

FIGURE 1.8: a) fibrinogen concentration (log) vs coagulation time (log) b) coagulation factor VIII concentration (log) vs coagulation time (log) (source: [11])

Another biosensor for fibrinogen detection is a piezoelectric agglutination sensor 1.9, (fibrinogen can transform fibrin through an agglutination reaction) presented in the work by Chen et al. [12]. The sensor is used to detect the fibrinogen agglutination reaction in

patients with coronary heart diseases: the density and viscosity of the reaction system change drastically during the course of agglutination. In addition, the standard curve between plasma agglutination time and fibrinogen concentration is established, in order to determinate fibrinogen content quantitatively. The fibrinogen concentration in coronary heart disease affected patients is significantly higher than that of the healthy control patients. The results reveal that high fibrinogen concentration is closely correlated to the occurrence, development and prognosis of coronary heart diseases. The determination can be completed within 10 minutes, showing that the device can be a good approach to real-time diagnostics, with other great advantages: small size, low cost and good precision.

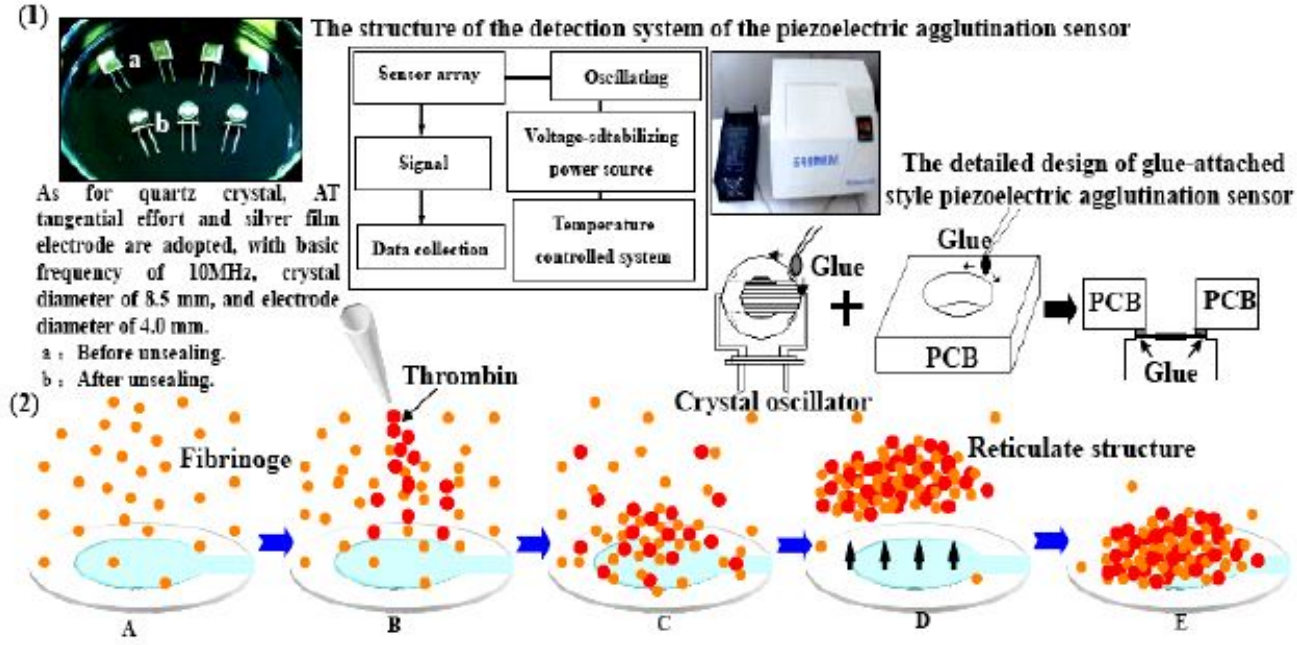

FIGURE 1.9: Piezoelectric agglutination sensor (source: [11])

A last example of nanotechnology based fibrinogen detection is presented in the work by Regmi et al. [13]. They designed an AlGaN/GaN HEMT for the direct detection of fibrinogen in human plasma; with such a device, the complex sample pre-treatment methods used in the traditional assays can be avoided. The test results in buffer solution and clinical plasma samples show high sensitivity, specificity, and dynamic range.

The sensor exhibits an ultra-low detection limit of $0.5\,\mathrm{g\,L^{-1}}$ and a detection range of $(0.5$ to $4.5)\,\mathrm{g\,L^{-1}}$ in 1 PBS with 1% BSA. The concentration dependent sensor signal in human serum samples demonstrates the specificity to fibrinogen in a highly dense matrix of background proteins. Results are obtained in 5 min with 5 µL sample volume: this sensing technique is ideal for speedy blood based diagnostics such as POC tests, homecare tests, or personalized healthcare.

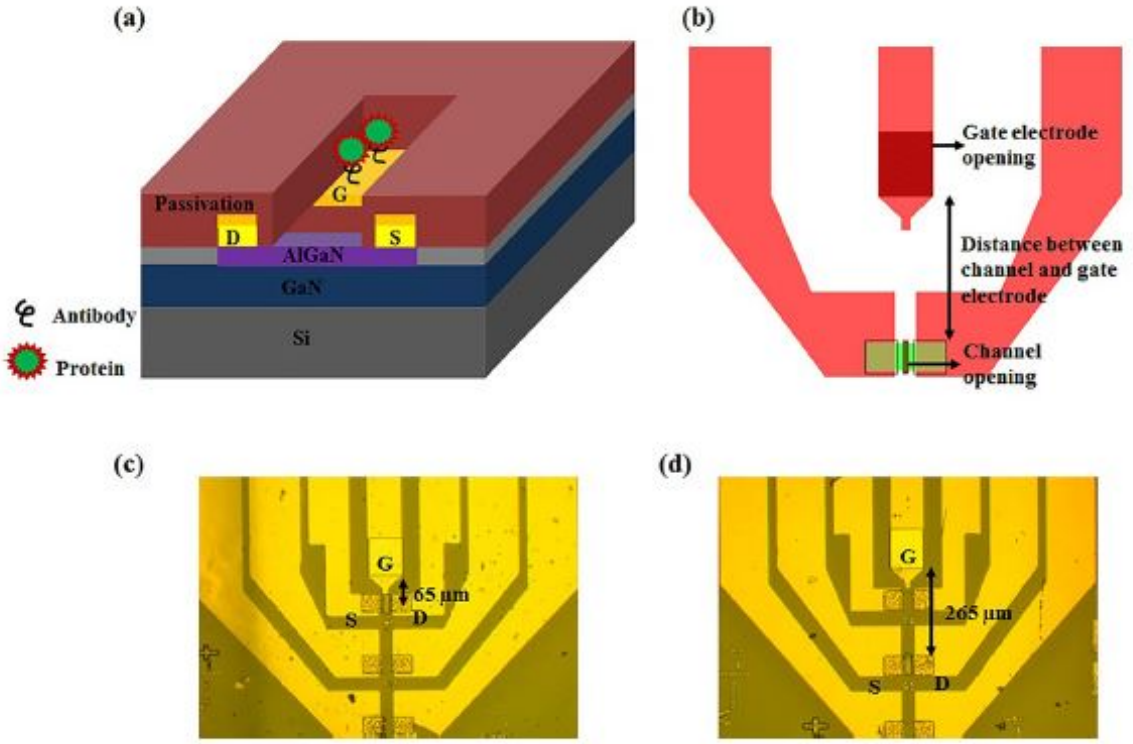

FIGURE 1.10: a) Schematic, b) layout and c)d) top views of the HEMT biosensor (source: [13])

Chapter 2

Chip fabrication

After having introduced in general nanogap and nanowire sensing devices, understanding their behavior and some of their applications, in this chapter it is described how the sensing device, here called "the chip", is made off and the fabrication process used to manufacture it. It is worth noting that some parts of its structure here are not used, because the design is inherited from a previous work [14].

The device is a square chip of around 5 mm^2. Due to its dimensions, the chip is wire bonded to a PCB (fig. 2.2) of some cm^2 to be better handled and to have an easier connection to the measuring instruments. The fabrication process is performed in two separate parts: first, a photo-lithographic step to create all the layers on the substrate and then a FIB milling to create the nanowire.

2.1 The device

The layout of the chip is showed in figure 2.1. The four vertical structures, made of gold, are the actual electrodes, used for sensing, and they are composed by a vertical pair of electrodes, with a nanowire bridging them, and two lateral ones; the latter were inherited from the previous work [14], where they were used as counter gates for the electromigration process. Note that the metallic tracks are spatially arranged in a particular way, to avoid problems of short circuits and thermal issues during the measurement. The width of these track goes from 300 µm to 1.5 µm: this was done to focus the electromigration used in the previous work in the center of the tracks; in this chip it is exploited

to have a sort of "rough" nanowire, before the FIB milling. After the milling the width is reduced from 1.5 µm to different widths, varying from 500 nm nm to 250 nm.

The top and down green squares are 300 µm pads, used for wire bonding, while the two squares near the electrodes (of the same dimensions of the other ones) were used, in the previous work, as reference electrodes and were made of platinum [14].

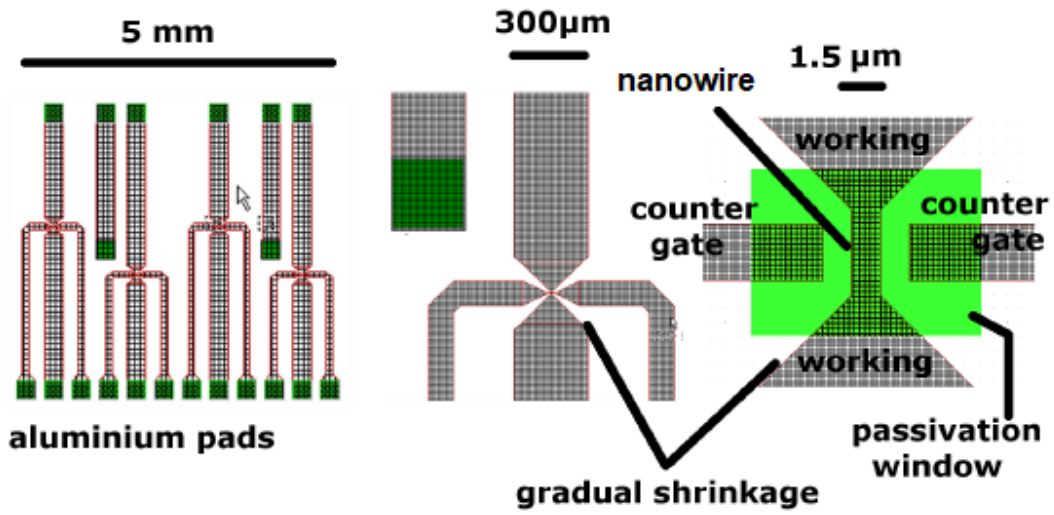

FIGURE 2.1: Chip layout. On the left the top view of the whole chip, in the center a detail of the elecrodes and on the right the nanowire and the passivation window. The width of the nanowire is reduced through FIB milling down to 0.5 µm

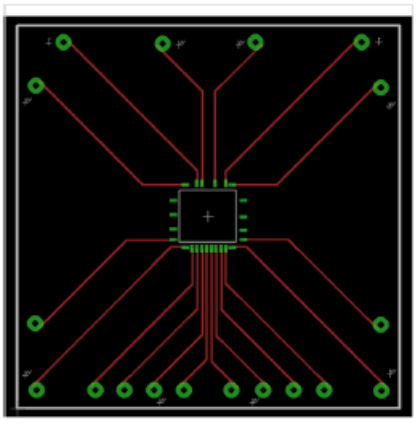

FIGURE 2.2: PCB Layout: the green spots are the contacts for the electronics and the red lines are the wires

The thickness of the metallic structures is 45 µm, 40 of gold + 5 of titanium, used as an adhesion layer. This low thickness gives a total resistance of the tracks of around (50 to 70) Ω at room temperature, smaller than the electrical resistance of the molecules used in the sensing process, that is typically around some MΩ.

2.2 Chip microfabrication

The lithographic process for the chip microfabrication is composed of different steps, represented in fig. 2.3:

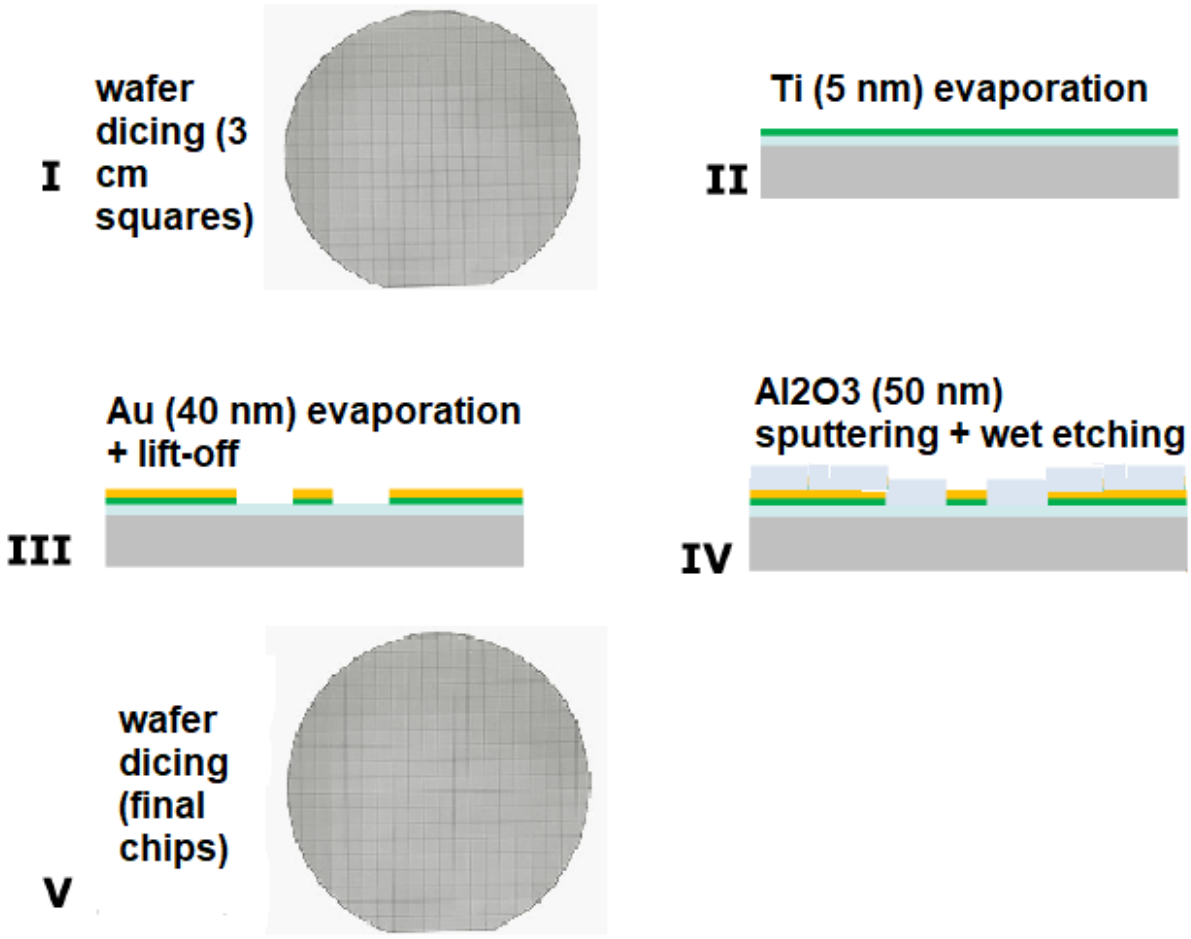

FIGURE 2.3: Microfabrication process starting from a SiO2 on Si wafer to the final sensing device. The lateral views represent the area around the bridges

2.2.1 Wafer dicing

The wafers used for this devices are SiO_2 on Si wafers,

- Silicon Wafers, CZ, Prime
- Diameter: 100 mm
- Type/Dopant: N/Phos
- Orientation: <1-0-0>
- Resistivity: $(1 \text{ to } 10)\,\Omega\,\text{cm}^{-1}$
- Thickness: $(525 \pm 25)\,\mu\text{m}$
- Oxide Thickness: 0.5 µm

supplied by Si-Mat [1].

After coating the wafer with a protective resist layer (around 1 µm), it is simply diced with a Disco Dicer, creating squares of 3 cm side, that are easier to be used in the photolithographic process, with respect to the whole wafer.

2.2.2 First photolithography

The first photolithographic step, preceded by a cleaning process to remove the dirt caused by the dicing, is performed previously to the Ti+Au evaporation and lift-off and it is composed by different steps.

- S1813 resist spinning (5 s @ 500 rpm + 50 s @ 5000 rpm)
- soft bake, 105 s @ 115°C
- UV light exposure for 4 s, through a glass-chromium mask, using a mask aligner (fig. 2.4)
- development with MF 319 developer for 60 s

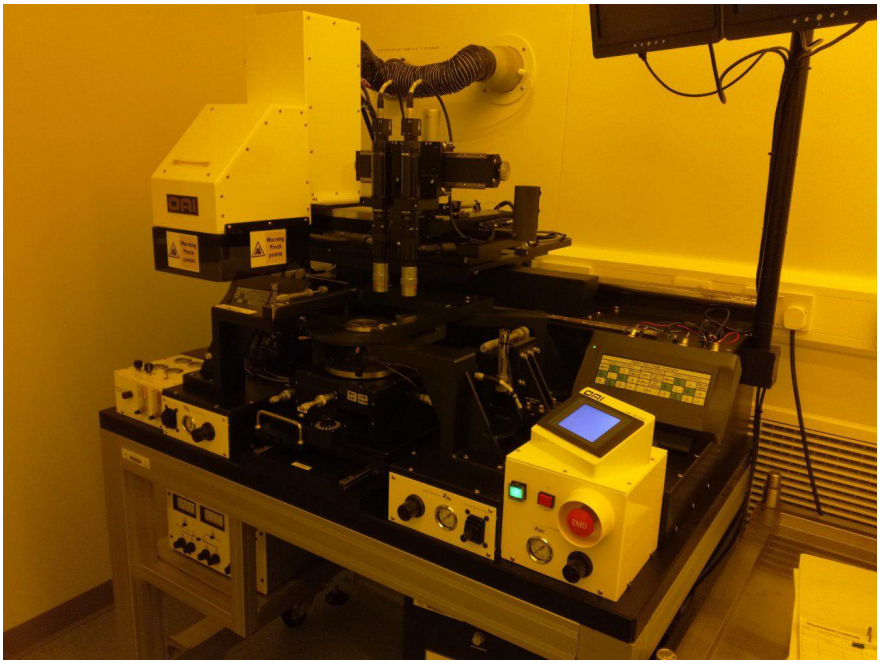

FIGURE 2.4: Mask aligner employed for photolithography

This particular lithography lead to some issues, given by the fact that the width of the smallest feature (i.e. the bridge between the electrodes) is around the sensitivity of S1813 resist: this makes very difficult to have the feature correctly done. To solve this problem, during the exposure a hard contact is performed between the sample and the mask.

The result of the lithography can be seen in figure 2.5

2.2.3 Titanium and gold evaporation and lift-off

Gold is employed for the electrodes due to his specific properties, like high conductivity and the ability to bond specific groups used for characterization; moreover, it is cheaper compared to other metals like platinum. Titanium is employed as an adhesion layer and it is preferred to other adhesion layers due to his low cost.

The evaporation is performed in a Temescal evaporator (fig. 2.6): the materials (Ti and Au) are deposited by electron beam evaporation (Temescal FC2000) in an high vacuum system (base pressure 8.0×10^{-8} mbar), pumped with a cryo-pump (CTI CT-8). The substrates are placed into a carousel. This system uses the intense beam of high energy

[1] https://www.si-mat.com/

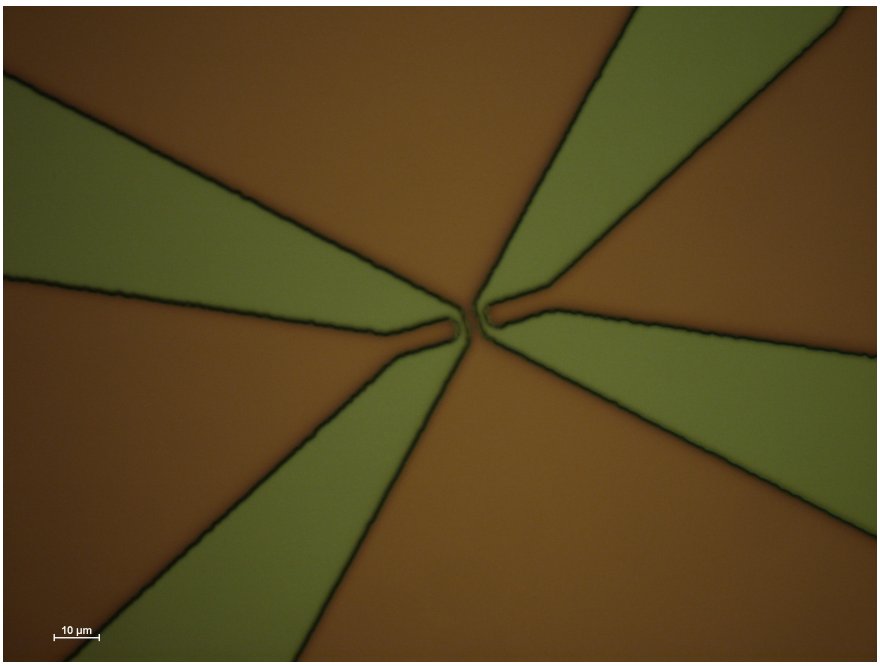

FIGURE 2.5: 100x image of the 1.5 µm x 3 µm bridge after the first photolithographic step

electrons to evaporate the source materials. The electrons are emitted from an hot filament and accelerated into the source material: this process can generate enough energy density to evaporate the material. The filament is located out of the evaporation cone, and the electron beam is directed to the material surface by a magnetic field. The electrical field accelerates the electrons and the magnetic field bends the electron beam of a 270° angle directly on the surface of the material. The electron beam can be rastered on the surface material to melt a significant amount of material. The source materials are usually contained into a crucible (called liner). The deposition rate is monitored using a quartz balance (Inficon) and fixed to $1\,\text{Å}\,\text{s}^{-1}$.

Then a lift-off with acetone follows, to remove the unwanted resist, titanium and gold.

2.2.4 Aluminum Oxide

The last layer composing the device is an Al_2O_3 passivation layer. The role of this passivation is double: to avoid short circuits during the measurements and to limit the effect of the electrolytic current, present in wet measurements.

FIGURE 2.6: Temescal FC2000 evaporator

Sputtering A 50 nm Aluminum Oxide layer is deposited through reactive RF magnetron sputtering on the devices. Power is set at 50 W during the entire process. In RF sputtering there is a cathode (the alumina) and a anode (the substrate). An impedance-matching network allows to transfer all the power from the RF source to the plasma discharge. The power supply is a high voltage RF source (13.56 MHz). The sputtering of an electrically insulating target become possible using RF-magnetron sputtering. The magnetron is a magnetically assisted discharge that improve the sputtering rate. The magnetic field concentrate the plasma in the space near the target, thus enhancing ion bombardment.

After the sputtering a second photolithographic step is performed. In this case the lithography is done after the deposition, because it is followed by an etching step instead of a lift-off like in the gold layer case. The lithographic steps are the same of the previous step:

- S1813 resist spinning (5 s @ 500 rpm + 50 s @ 5000 rpm)

- soft bake, 105 s @ 115°C
- UV light exposure for 4 s, through a glass-chromium mask
- development with MF 319 developer for 60 s

To remove the unwanted Al_2O_3, a wet etching process is performed: the samples are dipped in a 1% HF solution for 1 minute and then rinsed with DI water. Finally, the remaining resist is removed with aceton and IPA.

The result is shown in fig. 2.7: a window of 10 µm x 5 µm is created around the actual sensing area. Even the pads, that don't appear in the figure, are freed from the Al_2O_3 layer, to make possible the contacts with the measuring instrument.

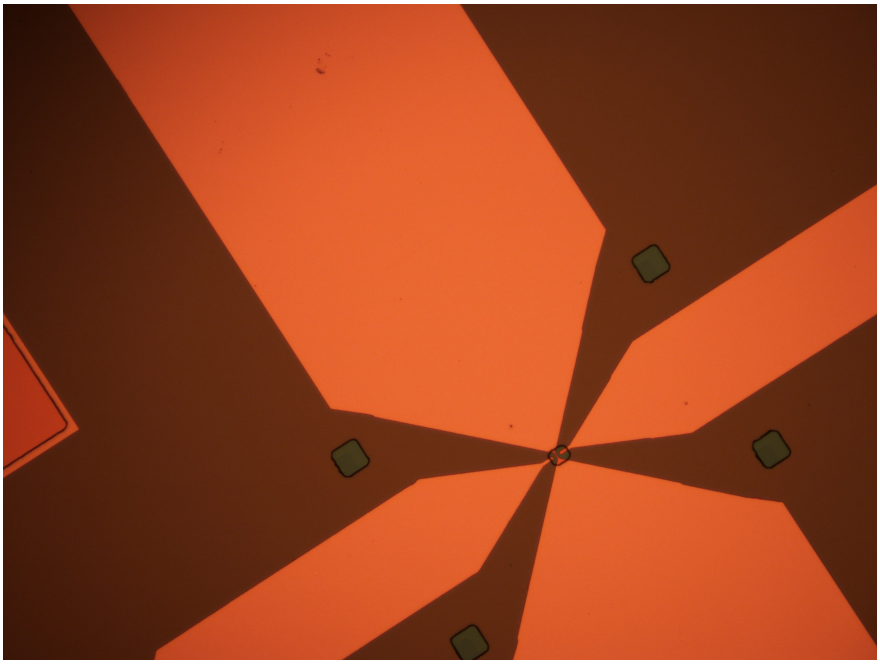

FIGURE 2.7: 20x image of the passivation windows on the device after the aluminum oxide sputtering and etching

The last step of the fabrication process is the final dicing from the 3cm-side squares to the actual chips. The squares are coated with a protective photoresist layer and then diced into the final devices, measuring around 5 mm^2. After the dicing the resist is removed with acetone and IPA.

2.3 FIB Milling

As written before, the width of the nanowires after the photolithographic process is 1.5 µm: to have a proper nanowire the width needs to be further reduced to less than 500 nm. This is impossible because of the limit of the photolithographic process, given by the sensitivity of the resist of about 1.3 µm, so a FIB milling is performed directly on the gold nanowires.

The instrument employed for the FIBbing is called NanoFab (fig. 2.8), manufactured by ORION [15] and it is composed by three different FIB ion guns: Gallium, Neon and Helium.

FIGURE 2.8: ORION Nanofab

The first tests are performed on some old devices, with the same features, to check what is the best ion gun to use for the milling. Helium is not working, because the area to be milled is to large: the helium is just swelling the surface and not sputtering the layers at all (fig. 2.9). Neon ion gun just give the same result.

Using Gallium ion, instead, a good milling is performed, giving an almost perfect gold nanowire. The milling is done on different devices, in order to have different widths and lengths for the measurements. In this way the most sensitive device can be found

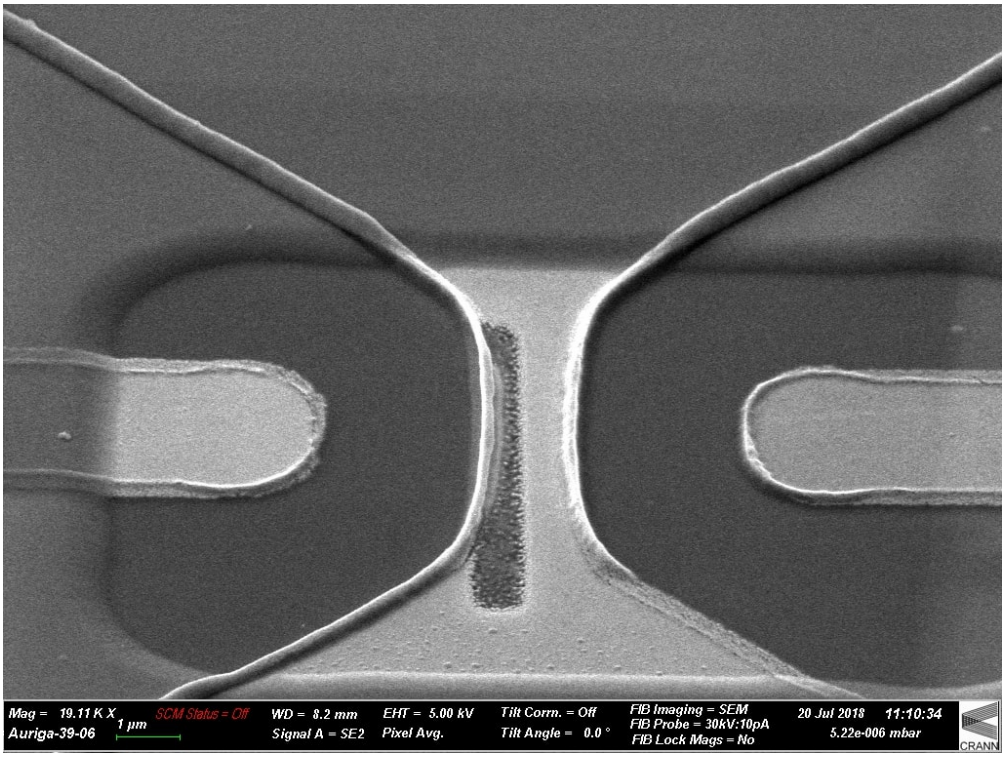

FIGURE 2.9: SEM image of a gold nanowire after Helium ion milling

comparing the resistance values found during the measurements. In the following, SEM images of the wire before the FIBbing and of some FIBbed gold nanowires are presented, to show the repeatability of the process on different devices and underline the difference of width between the "pre-FIBbed" and the FIBbed ones.

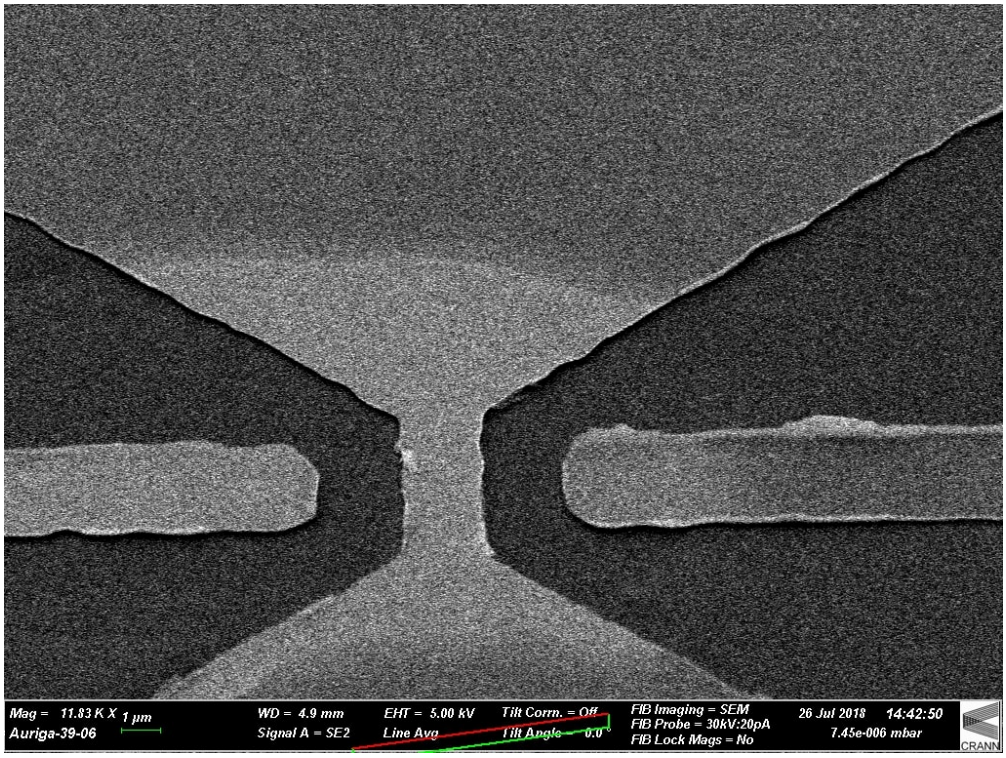

FIGURE 2.10: SEM image of a gold nanowire before Gallium ion milling. Width of the wire 1.5 µm, length of the wire 3 µm

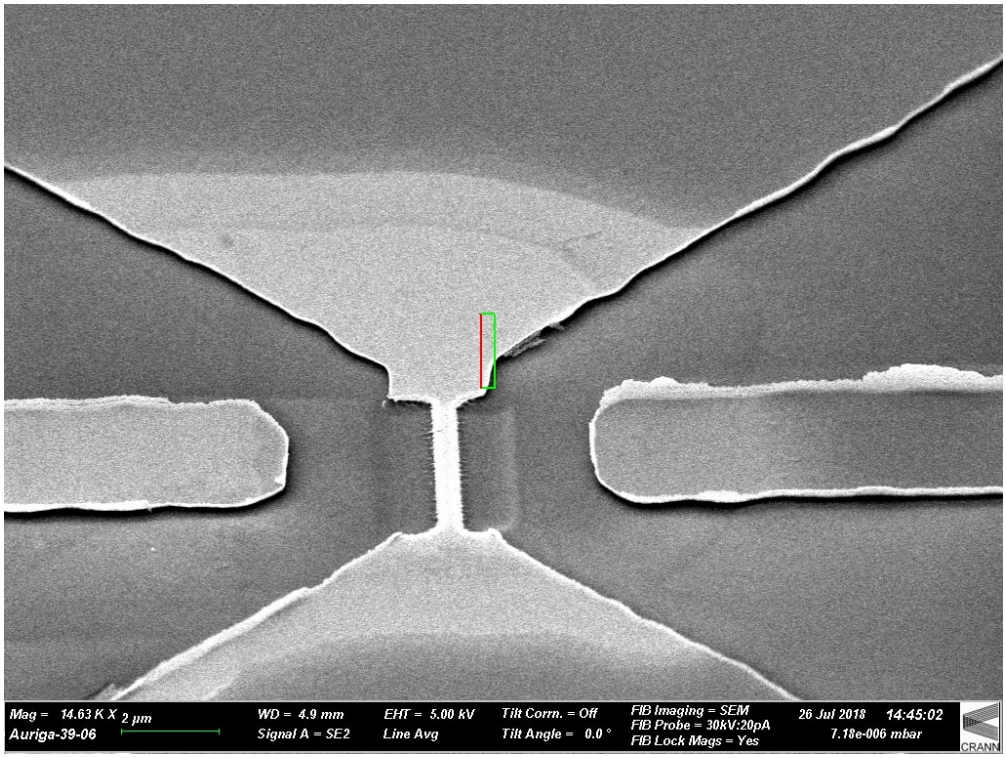

FIGURE 2.11: SEM image of a gold nanowire after Gallium ion milling. Width of the wire 0.5 µm, length of the wire 2.25 µm

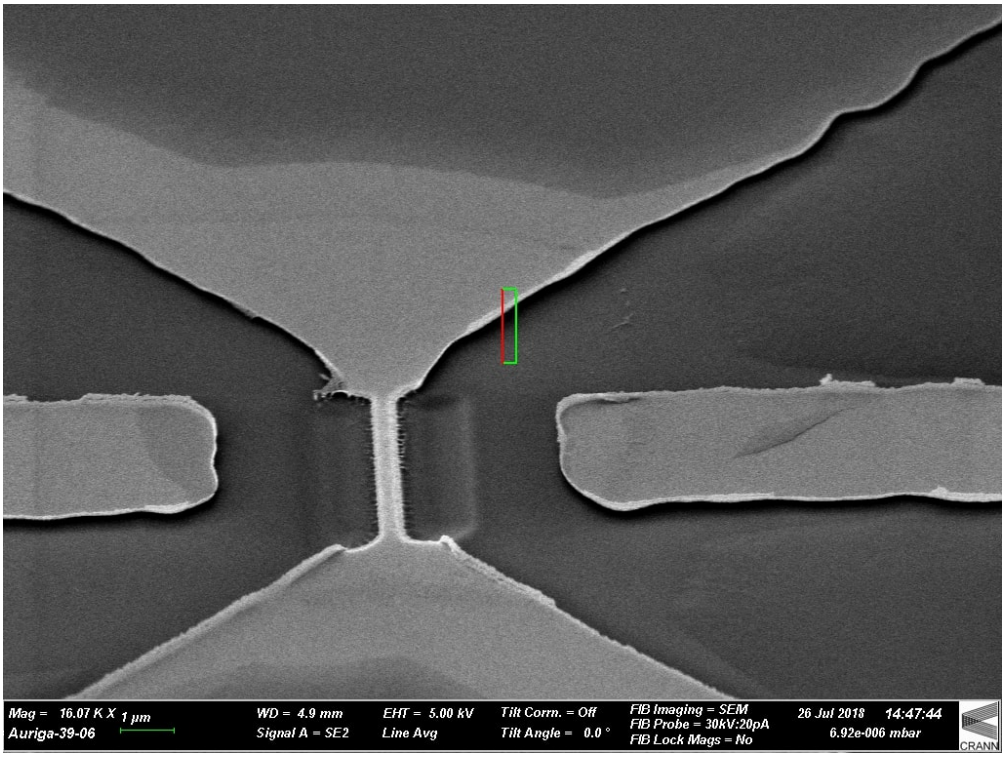

FIGURE 2.12: SEM image of a gold nanowire after Gallium ion milling. Width of the wire 0.5 µm, length of the wire 2.5 µm

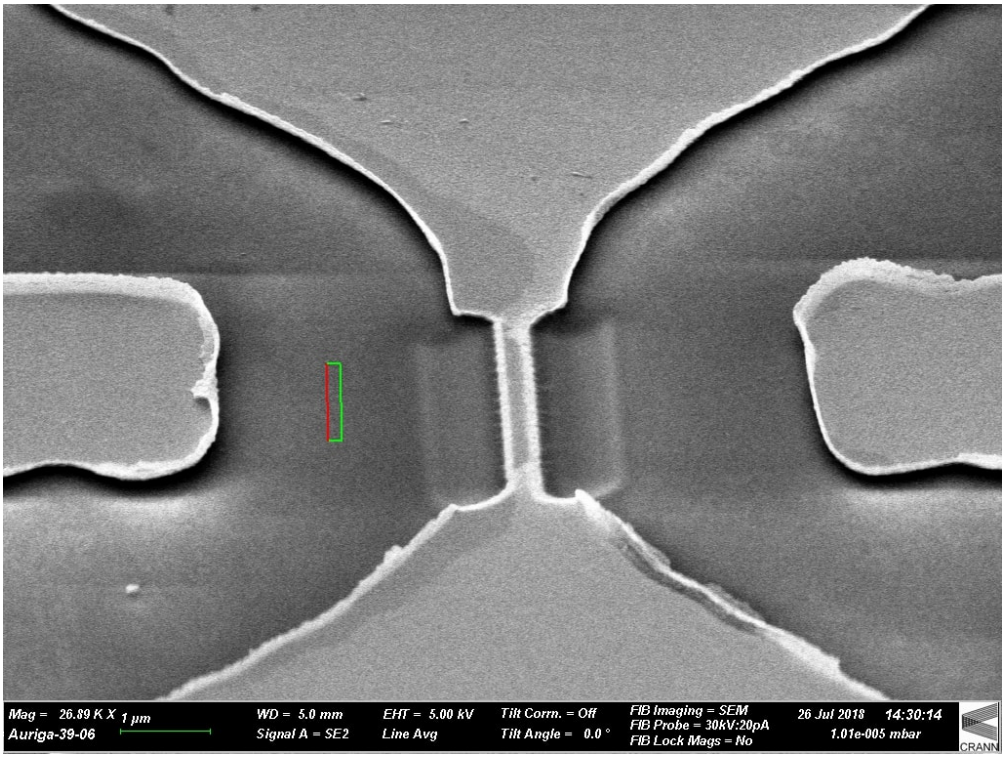

FIGURE 2.13: SEM image of a gold nanowire after Gallium ion milling. Width of the wire 0.4 µm, length of the wire 1.8 µm

Chapter 3

Biosensor testing and measurements

3.1 Experimental setup

After finishing the fabrication of the devices, the final step of the project is to perform measurements on the sensors: the devices are electrically stimulated (setting a DC current or a DC voltage) and then the resistance is measured through Ohm's law. Each measurement is repeated four times in order to have a statystical analysis and show the repeatability of the sensing. The analytes that will be measured are human fibrinogen, one of the glycoproteins present in human plasma, and a single droplet human blood sample, whose trombin molecules bind to the fibrinogen; knowing the values of the molecules involved in this reaction can serve as an indicator of infections, haemorrhaging [16] or even cancer [17].

Before starting the proper measurements of the analytes, a sensor calibration needs to be done, in order to establish what is the resistance of the bare nanowires. After three different measurements in air, in water and in PBS, a saline solution, the nanowires are functionalized through a proper surface modification. Finally a fibrinogen sample is added on the functionalized nanowires and then a single human blood droplet is put on the fibrinogen attached on the surface. By measuring the change in resistance between the different measuring steps a qualitative measurement is performed, in order to check if the sensor is able to correctly detect the presence fibrinogen and the bound between fibrinogen and the trombin molecules present in human plasma. To have a more precise evaluation of the operation of the devices, a sensing at different fibrinogen concentrations, followed

by a sensing of different human blood samples, needs to be performed; in this way a quantitative result can be obtained.

3.2 Sensor calibration

Before explaining the calibration of the devices, a clarification needs to be done. Due to an issue with the wire bonder, it was not possible to mount the devices on the PCBs prepared for that scope. Instead of tying the pads on the sensors to the PCB through metallic wires and then connect the pads on the PCB to a femto-amperometer, a probe station (fig. 3.1) is used to electrically stimulate the sensors: the pads on the devices are directly connected through metallic probes to the amperometer and to a computer where a specific LabView program is used to set the electrical stimulus and to take the results of the measurements.

FIGURE 3.1: Probe station employed for the measurements

3.2.1 Breakdown test and dynamic range

The first parameter that needs to be set is the maximum current for the measurements: since, as explained in [14], to trigger an electromigration in the middle of the gold bridge (considering a non-FIBbed device), a very high current density of $1 \times 10^8\,\mathrm{A\,cm^{-2}}$ is employed, the current to break the structure is around some tens of mAs. A "full" biosensor (not subject to the FIBbing process) is connected to the probe station and is stimulated to a current sweep in the range between 0.01 mA and 40 mA, with a step of 0.01 mA and a voltage compliance of 20 V; this last value is fundamental in order to avoid too high voltages and a breakdown of the measuring instrument. The resistance of the sensor remains constant until 33.15 mA, where it rises abruptly from 50 Ω to around 10 MΩ, with a drop of the current to less than 1 µA, showing a clear breaking of the gold bridge. The result of the measurement is shown in fig. 3.2

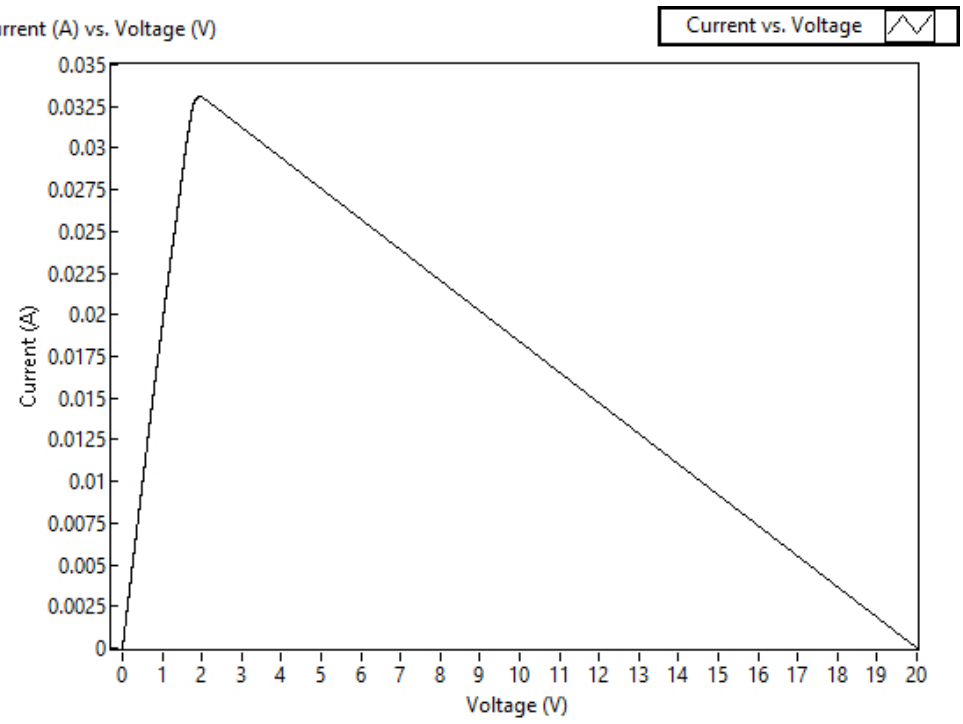

FIGURE 3.2: I/V curve of the breakdown test on a non-FIBbed device

Knowing this current limitation and knowing that the FIBbed devices are smaller and so they work with a lower current to avoid breakdown, a maximum operating current for the sensors is set to 10 µA.

There is no need to set a minimum operating current, but with too low current values the noise contribution is not negligible and it is affecting the measurements, so a minimum operating current is set to 0.1 µA.

3.2.2 Resistance of the sensor in air

The first resistance value to be measured is the resistance of the bare nanowire, i.e. the sensor without anything on top: as written before, the expected resistance value is around (50 to 100) Ω, depending on the dimensions of the FIBbed nanowires. A current sweep between 0.1 µA and 10 µA, with a step of 0.1 µA is set and the corresponding voltage is measured. The resistance values are calculated through Ohm's law and, together with the sensors' dimensions, are presented in table 3.1

TABLE 3.1: Resistance values of the sensors in air (sensor #0 is the non-FIBbed device). The resistance values are reported as a mean of 4 measurements, with the corresponding uncertainty

Sensor number	**Width (in μm)**	**Length (in μm)**	**Resistance (in Ω)**
#0	1.50	3.00	45.12 ± 2.34
#1	0.30	1.20	333.27 ± 2.59
#2	0.50	1.20	68.32 ± 1.83
#3	0.50	1.20	66.67 ± 0.41
#4	0.30	1.20	98.50 ± 1.02
#5	0.40	1.80	63.02 ± 1.85
#6	0.30	1.80	87.20 ± 1.23
#7	0.25	1.75	78.70 ± 0.68
#8	0.40	2.80	82.13 ± 3.43
#9	0.50	2.25	67.46 ± 0.24
#10	0.50	2.50	70.07 ± 0.71
#11	0.60	2.50	60.35 ± 1.18
#12	0.40	2.00	76.71 ± 0.17

All the sensors (unless #1 that will not be considered in the following steps) show a resistance in the range of (50 to 100) Ω and so they will be employed for the following measurements. One example of I/V curve is shown in figure 3.3: the values below 1 µA are too noisy and are not considered in the computation of the resistance.

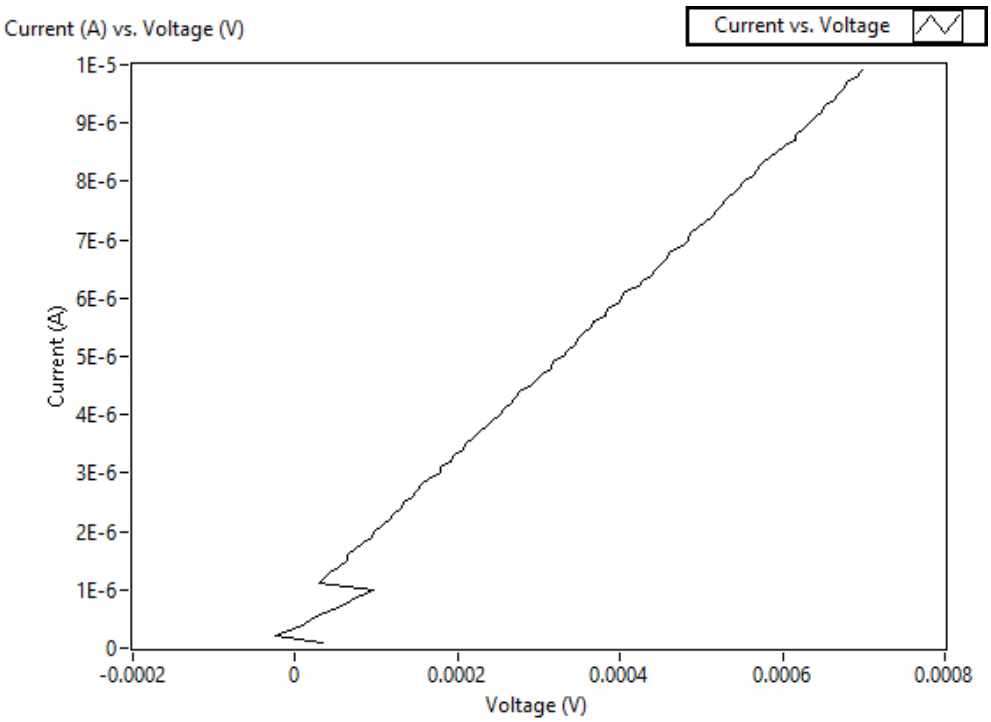

FIGURE 3.3: I/V curve of sensor #5 in air

3.2.3 Resistance of the sensor in water

Another resistance value that is important for the calibration of the sensor is the resistance of the nanowire when a small drop of DI water (around 1 µL of capacity) is put on top of it. This step is needed because the analytes that will be measured on the sensors are in aqueous solution, so a check of the correct functioning of the devices with water as a control analyte is crucial. The hypothesis to prove here is that the resistance value should not change, given that the DI water is apolar and thus will not have any charge transfer which could induce a change in the resistance. A current sweep between 0.1 µA and 10 µA, with a step of 0.1 µA, as in the previous measurement, is set and the corresponding voltage is measured. The resistance values are presented in table 3.2

Comparing these values with the values obtained in the previous step (table 3.1) it can be shown that the value of resistance changes in most of them, with a very high increase in sensors #7 #9 and #12. For the latter the value of resistance indicates a breakdown or a damage to the nanowire and so they will not be further taken into account for the measurements; for several other devices, instead, the change can be due to a non-perfect

TABLE 3.2: Resistance values of the sensors in water (device #0 is the non-FIBbed sensor). The resistance values are reported as a mean of 4 measurements, with the corresponding uncertainty

Senspr number	**Width (in μm)**	**Length (in μm)**	**Resistance (in Ω)**
#0	1.50	30	50.50 ± 0.35
#2	0.50	1.20	57.12 ± 1.13
#3	0.50	1.20	68.17 ± 2.02
#4	0.30	1.20	79.14 ± 3.42
#5	0.40	1.80	74.55 ± 0.97
#6	0.30	1.80	88.30 ± 0.71
#7	0.25	1.75	$224.56K \pm 0.55k$
#8	0.40	2.80	76.77 ± 1.21
#9	0.50	2.25	$145.45K \pm 0.78k$
#10	0.50	2.50	102.54 ± 3.45
#11	0.60	2.50	82.40 ± 3.14
#12	0.40	2.00	330.05 ± 0.89

quality of the water used for the test. One example of I/V curve is shown in figure 3.4: the values below 1 µA are again too noisy and are not considered in the computation of the resistance.

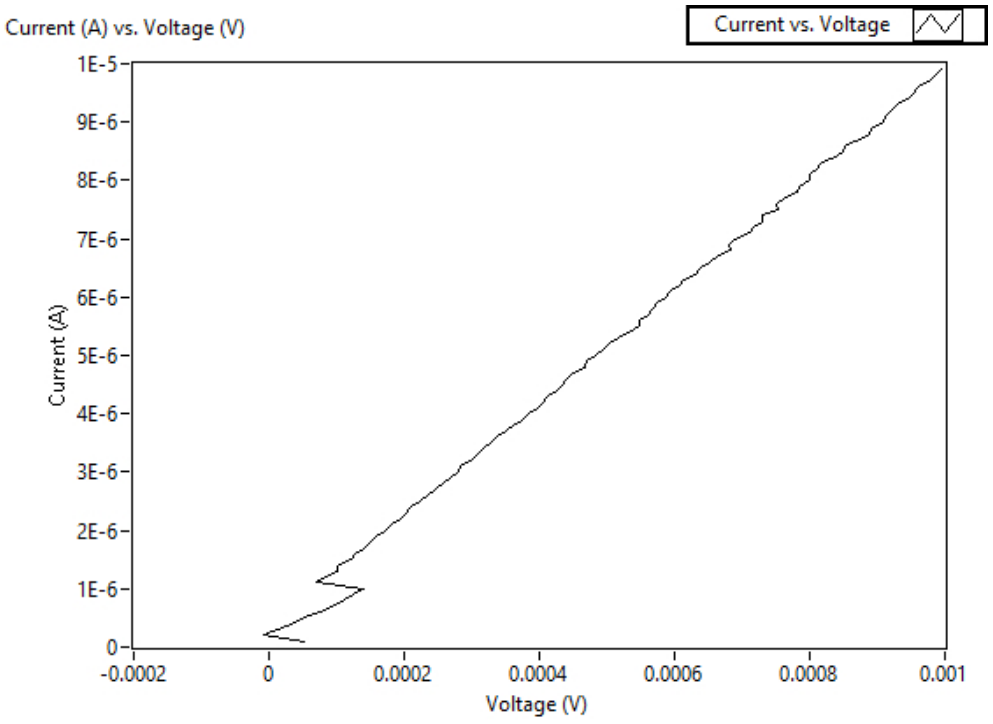

FIGURE 3.4: I/V curve of sensor #10 in water

3.2.4 Resistance of the sensor in PBS

The last step of the sensor calibration is the measurement of the resistance of the nanowires when a drop of PBS, a saline solution often employed in biological research, is put on the sensors. Since most of analytes used in this kind of research, like the fibrinogen employed in this work, are dissolved in PBS, a check of the resistance value can be useful in order to see if a solution different from DI water can introduce impurities on the gold surface, leading to a partial degradation and a change in resistance. A current sweep between 0.1 µA and 10 µA, with a step of 0.1 µA, as in the previous measurement, is set and the corresponding voltage is measured. The resistance values are presented in table 3.3

TABLE 3.3: Resistance values of the sensors in PBS (device #0 is the non-FIBbed device). The resistance values are reported as a mean of 4 measurements, with the corresponding uncertainty

Sensor number	**Width (in μm)**	**Length (in μm)**	**Resistance (in Ω)**
#0	1.50	3.00	68.16 ± 3.12
#2	0.50	1.20	62.24 ± 0.17
#3	0.50	1.20	70.66 ± 2.22
#4	0.30	1.20	122.16 ± 6.12
#5	0.40	1.80	85.65 ± 4.50
#6	0.30	1.80	106.29 ± 5.98
#8	0.40	2.80	101.2 ± 1.69
#10	0.50	2.50	73.04 ± 0.36
#11	0.60	2.50	85.38 ± 2.21

In this case the change in resistance is quite heterogeneous, due to the possible precipitation of salt on the gold surface. Some of the sensors show a decrease in resistance between the first measurement step and the second one or between second and third. This can be caused by some errors in the measurements or by some defects on the biosensors' surface. After this evaluation, sensor # 6 and # 11 are selected for the actual measurements, since they show a (not too high) increase of the resistance from the first step to the third one. An example of I/V curve of one of these two devices is shown in fig. 3.5.

The devices are then cleaned with acetone and IPA to remove all the possible impurities created by the PBS solution.

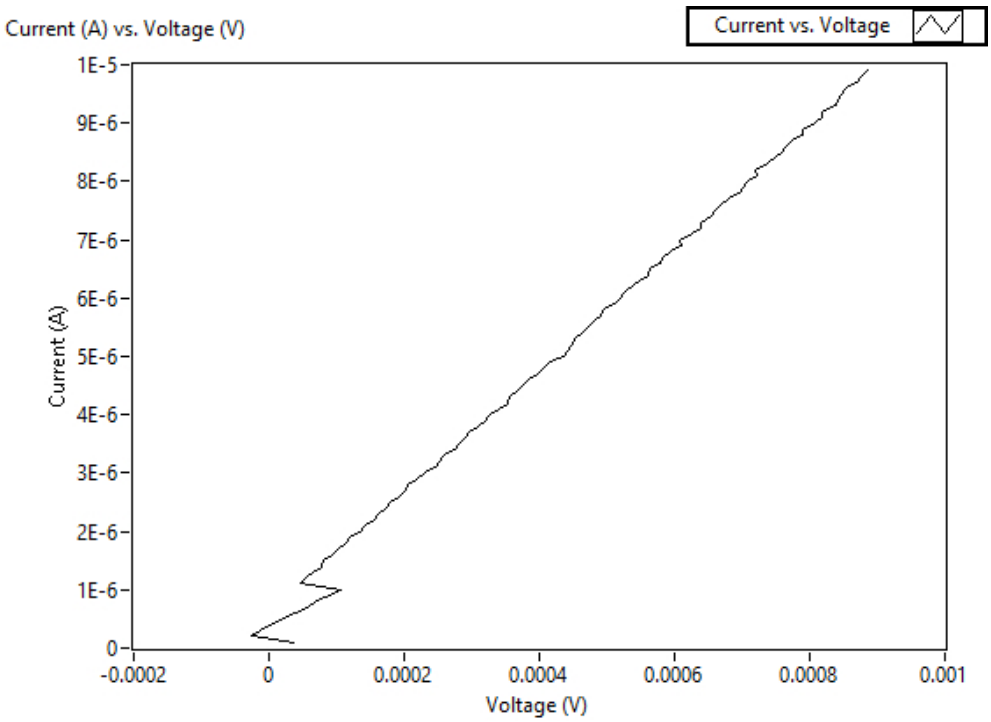

FIGURE 3.5: I/V curve of device #11 in PBS

3.3 Functionalization and sensor test

3.3.1 Surface functionalization

In order to perform a correct sensing of biomolecules, in our case fibrinogen, the surface of the gold nanowire should be functionalized; in this way the biomolecules are capable of binding to the nanowire surface. The functionalization process follows a protocol described by Arntz et al. [18]: the gold surface is covered by a 1 mM solution of DSU [19] in water-free 1, 4-dioxane for 1 hour, creating an amino-reactive surface that allows the fibrinogen molecules to attach to the surface. The working principle of this functionalization is shown in fig. 3.6: a DSU molecule is composed by two chains, that break when put in a dioxane solution. The -S group binds to gold surface and the other end of the chain is able to bind to the proteins that are put onto the device.

After drying the surface of the sample with nitrogen, the biosensor is put into the probe station to measure if the resistance changes after surface modification, as previously describe for the water and saline buffer. A current sweep between 0.1 µA and 10 µA, with a step of 0.1 µA, as in the previous measurement, is set and the corresponding voltage is

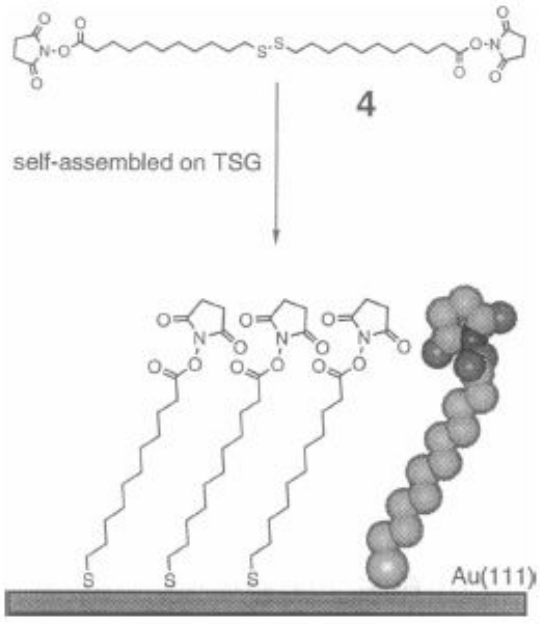

FIGURE 3.6: Self-assembled monolayer of DSU. Source: [19]

measured. The results of the measurements, using (as explained in section 3.2.4) sensors #6 and #11, are shown in table 3.4

TABLE 3.4: Resistance values of the sensors after gold functionalization. The resistance values are reported as a mean of 4 measurements, with the corresponding uncertainty

Sensor number	**Width (in μm)**	**Length (in μm)**	**Resistance (in Ω)**
#6	0.30	1.80	94.11 ± 0.56
#11	0.60	2.50	83.77 ± 0.41

As it can be seen comparing these values with the values in tab. 3.1, the resistance is increased with respect to the non-functionalized nanowire, as expected. In fact, the presence of the DSU on gold surface works as a degradation, changing the resistivity of the structure. This effect can be seen only in nanometric structures, like a gold thin film, because the thickness of the gold layer is not too big compared to the thickness of the functionalization on top of it. The I/V curves of the two sensors are reported in fig. 3.7 and 3.8

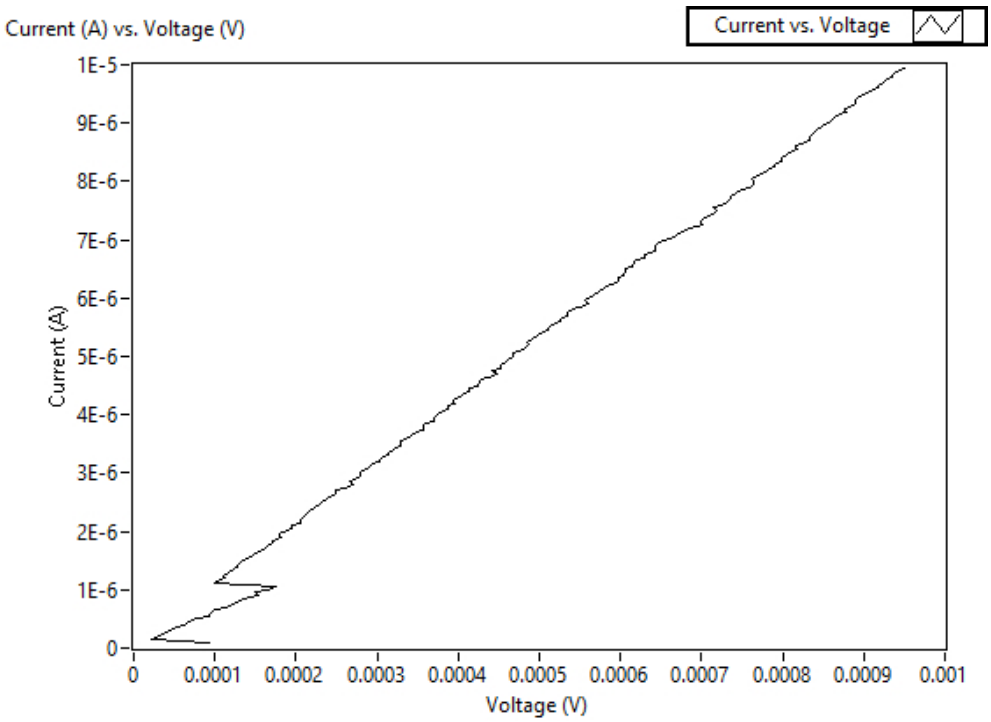

FIGURE 3.7: I/V curve of sensor #6 after functionalization

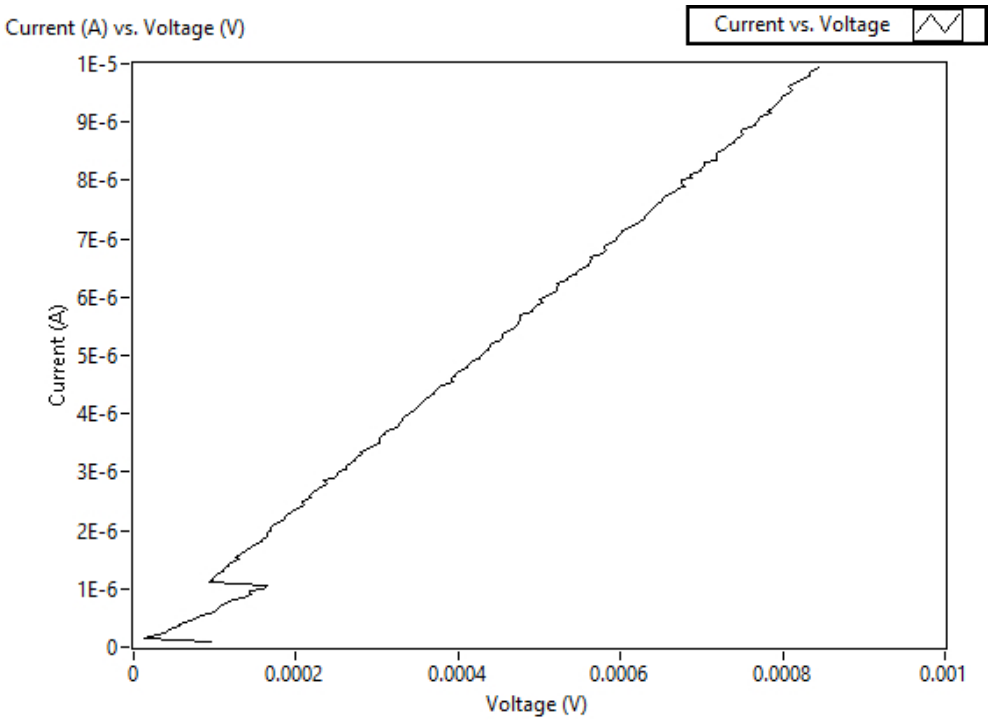

FIGURE 3.8: I/V curve of sensor #11 after functionalization

3.3.2 Fibrinogen measurement

A solution of fibrinogen in PBS, 100% concentration, is put on the functionalized sensors and let reacting for 20 minutes. The measurements are taken with the previously

explained current sweep and the resistance is calculated. The values are expected to increase with respect to the the previous ones because of the binding between the groups present on the functionalized surface and the proteins in the solution. The increase in the resistance indicates if the functionalization on the surface is good; unfortunately this kind of measurement is just qualitative and cannot indicate precisely the number of fibrinogen molecules. To do so, different fibrinogen concentrations should be measured and the sensor should be calibrated according to that measurements.

The resistance values calculated are shown in table 3.5

TABLE 3.5: Resistance values of the sensors after gold functionalization. The resistance values are reported as a mean of 4 measurements, with the corresponding uncertainty

Sensor number	**Width (in μm)**	**Length (in μm)**	**Resistance (in Ω)**
#6	0.30	1.80	145.75 ± 1.56
#11	0.60	2.50	84.08 ± 0.55

Comparing the values with the ones in table 3.4, it can be seen that fibrinogen molecules are binding quite strongly, with an increase in resistance of $51.64\,\Omega$, to device #6, while device #11 shows no increase in resistance. This can be due to different reasons:

- fibrinogen molecules did not bind to the functionalization, even if this was carefully and precisely carry out
- fibrinogen molecules did not bind to the functionalization, because the functionalization did not work properly
- a very small portion of fibrinogen molecules bound to the functionalization, so that the change in resistance is negligible

I/V curves for the two sensors are shown in fig. 3.9 and 3.10

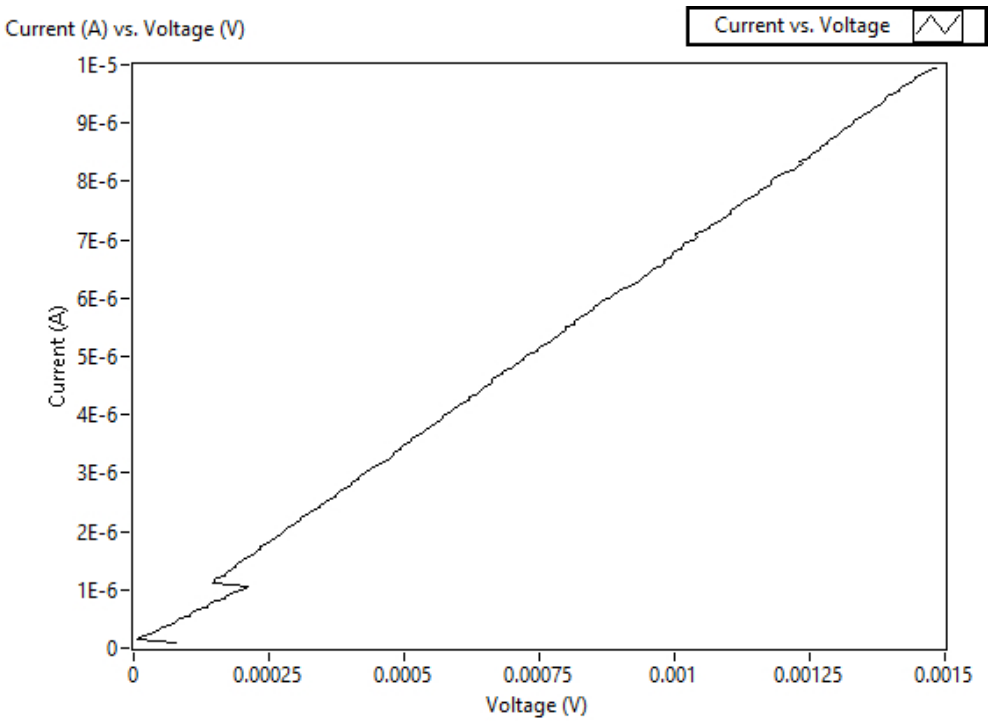

FIGURE 3.9: I/V curve of sensor #6 with fibrinogen on it

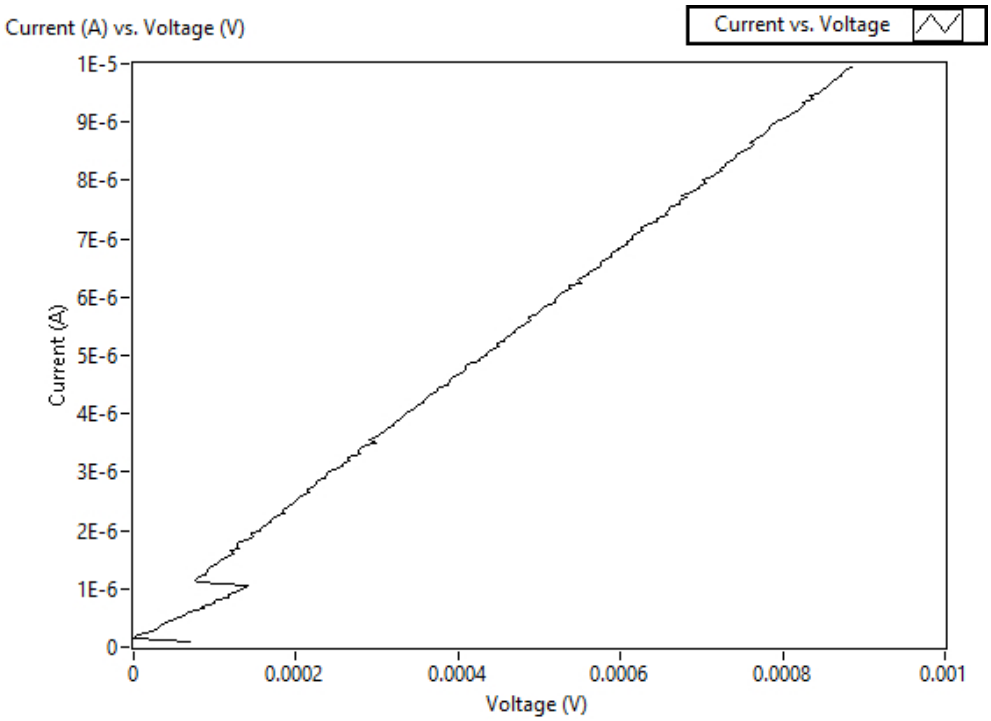

FIGURE 3.10: I/V curve of sensor #11 with fibrinogen on it

3.3.3 Result validation through blood detection

To have a validation of this results and check if there was really a binding event on the nanowire surface, a single full blood droplet is put on the device surface (without removing the fibrinogen). In this way, since the fibrinogen has the capability to bind to monocytes present in human blood [20], if a change of resistance is detected it means that a binding event happens between monocytes and fibrinogen molecules.

For this last set of measurements, a lower current is employed, since the sensors were probably ruined by the continuous tests and by the different substances put on top of them. The current sweep is set from 0.1 µA to 1 µA, with a step of 0.05 µA and the corresponding voltage is measured. The values of the resistances calculated are shown in table 3.6

TABLE 3.6: Resistance values of the nanowire devices after binding between fibrinogen and blood. The resistance values are reported as a mean of 4 measurements, with the corresponding uncertainty

Sensor number	**Width (in μm)**	**Length (in μm)**	**Resistance (in Ω)**
#6	0.3	1.8	674.75 ± 3.87
#11	0.6	2.5	90.85 ± 0.51

The results confirm the values obtain in section 3.3.2. For sensor #6 the fibrinogen bound strongly to the surface and the presence of blood is detected through a huge increase in resistance; for sensor #11 the increase in resistance is small, meaning a bad attachment of the fibrinogen molecules to the surface.

The I/V curves for the two biosensors are shown in fig. 3.11 and 3.12:

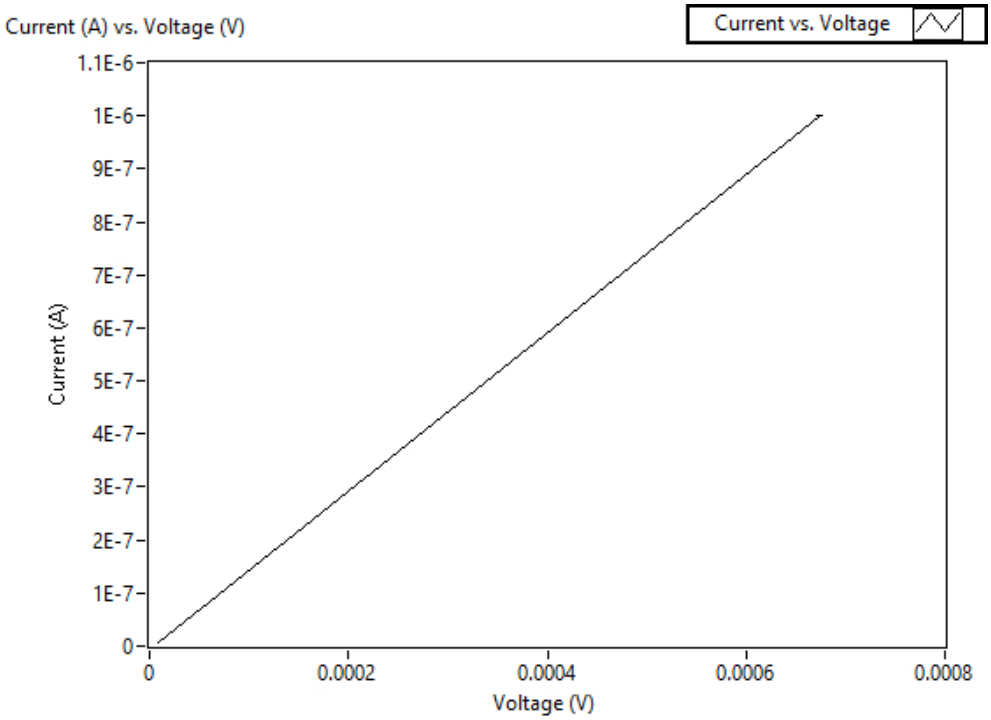

FIGURE 3.11: I/V curve of sensor #6 with fibrinogen and blood on it

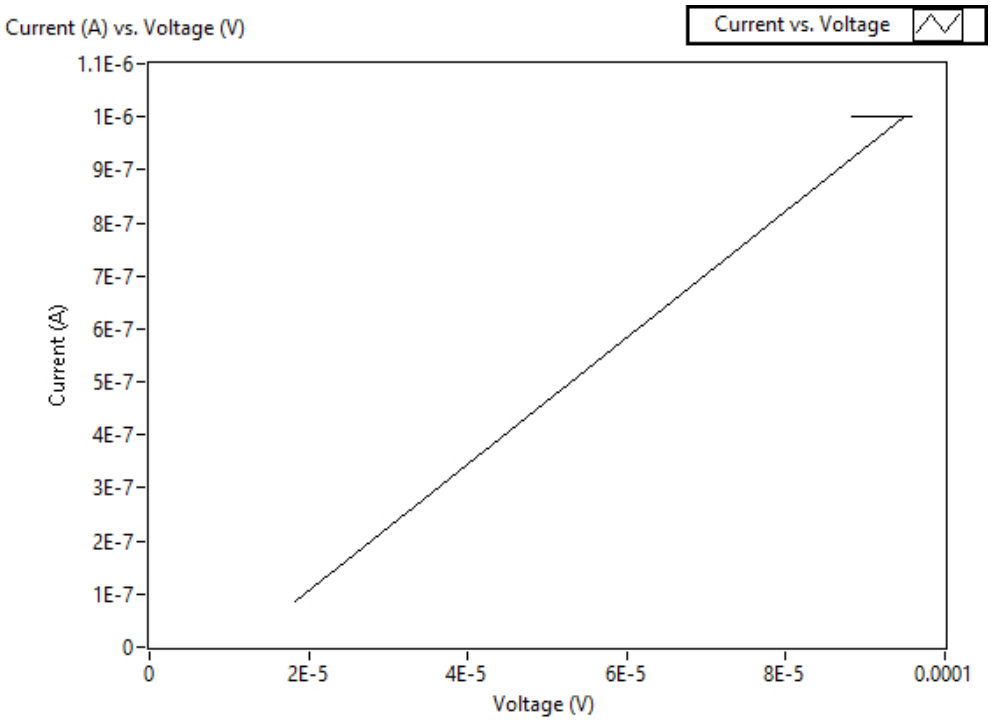

FIGURE 3.12: I/V curve of sensor #11 with fibrinogen and blood on it

Chapter 4

Conclusion: analysis of the results, final remarks, outlook and future work

4.1 Results analysis

4.1.1 Summary

The results presented in chapter 3 are here resumed in table 4.1, in order to make a direct comparison between the two different devices analyzed:

TABLE 4.1: Summary of the resistance values of the sensors #6 and #11

Sensor number	**Width**	**Length**	**Resistance in air**
#6	0.30 µm	1.80 µm	87.2 Ω
#11	0.60 µm	2.50 µm	60.35 Ω
Sensor number	**Resistance in water**	**Resistance in PBS**	**Resistance after func.**
#6	88.30 Ω	106.29 Ω	94.11 Ω
#11	82.4 Ω	85.38 Ω	83.77 Ω
Sensor number	**Resistance with fibr.**	**Resistance with blood**	
#6	145.75 Ω	674.75 Ω	
#11	84.08 Ω	90.85 Ω	

From the table it can be noticed that the smaller device shows a better response to functionalization and fibrinogen biosensing, with a moderate increase in resistance. For

the bigger device the resistance measured when performing the biomolecule measurement is left almost unchanged. This can be due to a failure in the functionalization or to a lack of sensitivity, caused by the bigger dimensions of the nanowire.

4.1.2 Result analysis

As explained in the previous sections, the aim of this project is to design a nanowire-based biosensor, with a cost-effective solution: it can be concluded that the work was successful, because the results obtained from the measurements are promising. In fact they show that the sensors can actually detect biomolecules in aqueous solution put on the gold surface. The results show also that the best sensitivity is reached working with smaller nanowires. Regarding the cost-effectiveness, all the materials employed for the devices are standards in fabrication and so quite cheap and also the techniques employed (photolithography and FIBbing) are present in most labs and are easy to perform.

It is important to underline that it is difficult to find similar analyses, due to the fact that this kind of analysis performed on the sensors is unique.

In order to have a more precise evaluation of the phenomenon, further work needs to be done, that will be explained in next section.

4.2 Future work

The work done during my project validated the correct functioning of the sensors as biosensing platform for the detection of fibrinogen. Probably they can be also used to detect other proteins present in human bodies, like immunoglobuline. Some further work needs to be done, in order to have a correct sensor calibration for the specific molecules that needs to be detected and to have quantitative measurements.

To do the calibration of the sensor, correlating different fibrinogen concentrations to different change in resistances, one approach that can be followed is the use of an ELISA kit standard curve. In this kind of detection instruments, different concentrations of fibrinogen are put into plates and the proteins are linked to light-reacting enzymes: for each

concentration, the corresponding optical density is detected through a specific instrument, that is able to sense the light emitted by the enzymes, and the standard curve is built 4.1.

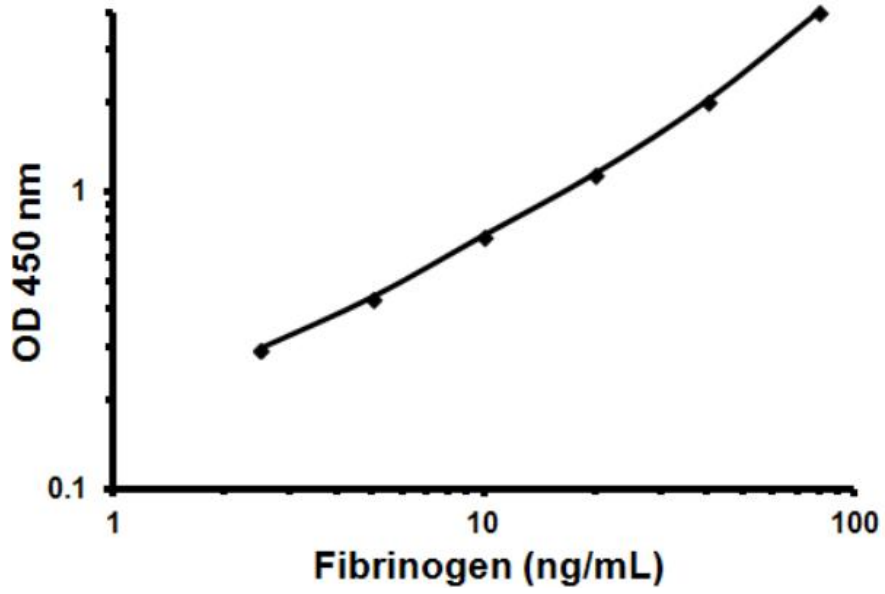

FIGURE 4.1: Example of a standard curve for a fibrinogen ELISA kit. Source: [21]

After doing the ELISA assay, the same concentrations are measured through the nanowire biosensor and a similar standard curve is built, with the resistance on the y-axis, instead of the O.D.

Another step that should be taken forward, following the calibration, is the detection of fibrinogen levels in different human blood samples, some of them taken from unhealthy people. In this way, using the standard curve of the sensor, different fibrinogen levels can be detected in real time, in order to obtain information about the health state of the patients.

Bibliography

[1] Xing Chen et al. “Electrical nanogap devices for biosensing”. In: *Materials Today* 13.11 (2010), pp. 28 –41. ISSN: 1369-7021.

[2] Somenath Roy et al. “Direct Electrical Measurements on Single-Molecule Genomic DNA Using Single-Walled Carbon Nanotubes”. In: *Nano Letters* 8.1 (2008), pp. 26–30.

[3] Sang Kyu Kim et al. “Nanogap biosensors for electrical and label-free detection of biomolecular interactions”. In: *Nanotechnology* 20.45 (2009), p. 455502.

[4] Gregory S. McCarty, Benjamin Moody, and Matthew K. Zachek. “Enhancing electrochemical detection by scaling solid state nanogaps”. In: *Journal of Electroanalytical Chemistry* 643.1 (2010), pp. 9 –14. ISSN: 1572-6657.

[5] Somenath Roy et al. “Mass-Produced Nanogap Sensor Arrays for Ultrasensitive Detection of DNA”. In: *Journal of the American Chemical Society* 131.34 (2009), pp. 12211–12217.

[6] Maya Zayats et al. “Biocatalytic Growth of Au Nanoparticles: From Mechanistic Aspects to Biosensors Design”. In: *Nano letters* 5 (Feb. 2005), pp. 21–5.

[7] Yashuang Lu et al. “Enzyme-functionalized gold nanowires for the fabrication of biosensors”. In: *Bioelectrochemistry* 71.2 (2007), pp. 211 –216. ISSN: 1567-5394.

[8] Jianing Hui et al. “A High Throughput Glucose Biosensor Based on FIA and Gold Nanowire Arrays at Low Potential”. In: *Journal of The Electrochemical Society* 161 (Sept. 2014), pp. 291–296.

[9] Li Guicai et al. “Investigation of fibrinogen adsorption on solid surface by quartz crystal microbalance with dissipation(QCM-D) and ELISA”. In: *Solid State Ionics* 179.21 (2008). Solid State Ionics 16: Proceedings of the 16th International Conference on Solid State Ionics (SSI-16), Part I, pp. 932 –935. ISSN: 0167-2738.

[10] Kelvin W. C. Poon et al. “Quantitative reagent-free detection of fibrinogen levels in human blood plasma using Raman spectroscopy”. In: *Analyst* 137 (8 2012), pp. 1807–1814.

[11] Chunyan Yao, Ling Qu, and Weiling Fu. “Detection of Fibrinogen and Coagulation Factor VIII in Plasma by a Quartz Crystal Microbalance Biosensor”. In: *Sensors* 13.6 (2013), pp. 6946–6956. ISSN: 1424-8220.

[12] Ming Chen et al. "Quantitative Determination of Fibrinogen of Patients with Coronary Heart Diseases through Piezoelectric Agglutination Sensor". In: *Sensors* 10 (Mar. 2010).

[13] Abiral Regmi et al. "Direct detection of fibrinogen in human plasma using electric-double-layer gated AlGaN/GaN high electron mobility transistors". In: *Applied Physics Letters* 111 (Aug. 2017), p. 082106.

[14] Ismael Rattalino. "Nanogap electrodes for molecular electronics and biosensing". PhD thesis. Politecnico di Torino, 2014.

[15] *ORION NanoFab*. URL: https://www.zeiss.com/semiconductor-manufacturing-technology/products-solutions/process-control-solutions/orion-nanofab-multi-ion-fib.html.

[16] Dimitrios Davalos and Katerina Akassoglou. "Fibrinogen as a key regulator of inflammation in disease". In: *Semin Immunopathol* 34.1 (2012), pp. 34 –43.

[17] Ombretta Repetto and Valli De Re. "Coagulation and fibrinolysis in gastric cancer". In: *Annals of the New York Academy of Sciences* 1404 (2017), pp. 27 –48.

[18] Y Arntz et al. "Label-free protein assay based on a nanomechanical cantilever array". In: *Nanotechnology* 14.1 (2003), p. 86.

[19] Peter Wagner et al. "Covalent immobilization of native biomolecules onto Au(111) via N-hydroxysuccinimide ester functionalized self-assembled monolayers for scanning probe microscopy". In: *Biophysical journal* 70 (June 1996), pp. 2052–66.

[20] D C Altieri, P M Mannucci, and A M Capitanio. "Binding of fibrinogen to human monocytes". In: *The Journal of Clinic Investigation* 78.4 (1986), pp. 968–976.

[21] *Human Fibrinogen ELISA Kit (ab108841)*. 2018. URL: https://www.abcam.com/human-fibrinogen-elisa-kit-ab108841.html.